CACHD1 is an α2δ-like protein that modulates CaV3 voltage-gated calcium channel activity

Article

Accepted Version

Cottrell, G. S. ORCID: https://orcid.org/0000-0001-9098-7627, Soubrane, C. H., Hounshell, J. A., Lin, H., Owenson, V., Rigby, M., Cox, P. J., Barker, B. S., Ottolini, M., Ince, S., Bauer, C. C., Perez-Reyes, E., Patel, M. K., Stevens, E. B. and Stephens, G. J. ORCID: https://orcid.org/0000-0002-8966-4238 (2018) CACHD1 is an α2δ-like protein that modulates CaV3 voltage-gated calcium channel activity. The Journal of Neuroscience, 38 (4). pp. 9186-9201. ISSN 1529-2401 doi: https://doi.org/10.1523/JNEUROSCI.3572-15.2018 Available at https://centaur.reading.ac.uk/79082/

To link to this article DOI: http://dx.doi.org/10.1523/JNEUROSCI.3572-15.2018

Publisher: The Society for Neuroscience

JNeurosci
THE JOURNAL OF NEUROSCIENCE

Research Articles: Cellular/Molecular

CACHD1 is an α2δ-like protein that modulates Ca_V3 voltage-gated calcium channel activity

Graeme S. Cottrell[1], Camille H. Soubrane[1], James A. Hounshell[3,5], Hong Lin[1], Venetia Owenson[2], Michael Rigby[2], Peter J. Cox[2], Bryan S. Barker[3,5], Matteo Ottolini[3], Selvi Ince[1], Claudia C. Bauer[1], Edward Perez-Reyes[4,5], Manoj K. Patel[3,5], Edward B. Stevens[2] and Gary J. Stephens[1]

[1]University of Reading, Whiteknights Campus, Reading, RG6 6AJ.

[2]Pfizer Neuroscience and Pain Research Unit, Portway Building, Granta Park, Great Abington, Cambridge, CB21 6GS.

[3]Departments of Anesthesiology

[4]Pharmacology

[5]Neuroscience Graduate Program, University of Virginia, Charlottesville, VA, USA, 22908

DOI: 10.1523/JNEUROSCI.3572-15.2018

Received: 22 September 2015

Revised: 3 June 2018

Accepted: 13 June 2018

Published: 4 September 2018

Author contributions: G.S.C., C.H.S., J.H., P.C., E.P.-R., M.K.P., E.B.S., and G.J.S. designed research; G.S.C., C.H.S., J.H., H.L., V.O., B.S.B., M.O., S.I., C.b., and M.K.P. performed research; G.S.C., C.H.S., J.H., H.L., M.R., B.S.B., and M.K.P. analyzed data; C.H.S., M.K.P., E.B.S., and G.J.S. wrote the paper; P.C., E.P.-R., E.B.S., and G.J.S. contributed unpublished reagents/analytic tools.

Conflict of Interest: The authors declare no competing financial interests.

Work supported by a BBSRC Departmental Training Grant award with CASE award from Pfizer UK to GJS and EBS to support CHS. This work was also supported by NIH/NINDS grant NS075157 to MKP and NIH grant NS069524 to EPR.

Corresponding authors: Gary J. Stephens, School of Pharmacy, University of Reading, Whiteknights, PO Box 228, Reading RG6 6AJ, UK. E-mail: g.j.stephens@reading.ac.uk Edward B Stevens, Pfizer Neuroscience and Pain Research Unit, Portway Building, Granta Park, Cambridge, CB21 6GS, UK. Email: edward.stevens@metrionbiosciences.com.

Cite as: J. Neurosci ; 10.1523/JNEUROSCI.3572-15.2018

CACHD1 is an α2δ-like protein that modulates $\mathrm{Ca_V3}$ voltage-gated calcium channel activity

Abbreviated title: CACHD1 modulation of $\mathrm{Ca_V3}$ channels

Graeme S. Cottrell[1*], Camille H. Soubrane[1*], James A. Hounshell[3,5], Hong Lin[1], Venetia Owenson[2], Michael Rigby[2], Peter J. Cox[2], Bryan S. Barker[3,5], Matteo Ottolini[3], Selvi Ince[1], Claudia C. Bauer[1], Edward Perez-Reyes[4,5], Manoj K. Patel[3,5], Edward B. Stevens[2], Gary J. Stephens[1]

[1]University of Reading, Whiteknights Campus, Reading, RG6 6AJ.

[2]Pfizer Neuroscience and Pain Research Unit, Portway Building, Granta Park, Great Abington, Cambridge, CB21 6GS.

Departments of [3]Anesthesiology, [4]Pharmacology, and [5]Neuroscience Graduate Program, University of Virginia, Charlottesville, VA, USA, 22908.

*These authors contributed equally to this work.

Corresponding authors:

Gary J. Stephens, School of Pharmacy, University of Reading, Whiteknights, PO Box 228, Reading RG6 6AJ, UK. E-mail: g.j.stephens@reading.ac.uk.

Edward B Stevens, Pfizer Neuroscience and Pain Research Unit, Portway Building, Granta Park, Cambridge, CB21 6GS, UK. Email: edward.stevens@metrionbiosciences.com.

Number of pages: 46

Number of figures: 9; tables: 2

Number of words for Abstract (191), Introduction (429), and Discussion (1561)

Acknowledgements

Work supported by a BBSRC Departmental Training Grant award with CASE award from Pfizer UK to GJS and EBS to support CHS. This work was also supported by NIH/NINDS grant NS075157 to MKP and NIH grant NS069524 to EPR.

Abstract

The putative cache (Ca^{2+} channel and chemotaxis receptor) domain containing 1 (CACHD1) protein has predicted structural similarities to members of the $\alpha 2\delta$ voltage-gated Ca^{2+} channel (VGCC) auxiliary subunit family. CACHD1 mRNA and protein were highly expressed in the male mammalian CNS, in particular in the thalamus, hippocampus and cerebellum, with a broadly similar tissue distribution to Ca_V3 subunits, in particular, $Ca_V3.1$. In expression studies, CACHD1 increased cell-surface localization of $Ca_V3.1$ and these proteins were in close proximity at the cell surface consistent with the formation of CACHD1-$Ca_V3.1$ complexes. In functional electrophysiological studies, co-expression of human CACHD1 with $Ca_V3.1$, $Ca_V3.2$ and $Ca_V3.3$ caused a significant increase in peak current density and corresponding increases in maximal conductance. By contrast, $\alpha 2\delta$-1 had no effect on peak current density or maximal conductance in either $Ca_V3.1$, $Ca_V3.2$ or $Ca_V3.3$. Comparison of CACHD1-mediated increases in $Ca_V3.1$ current density and gating currents revealed an increase in channel open probability. In hippocampal neurons from male and female E19 rats, CACHD1 overexpression increased Ca_V3-mediated action potential (AP) firing frequency and neuronal excitability. These data suggest that CACHD1 is structurally an $\alpha 2\delta$-like protein that functionally modulates Ca_V3 voltage-gated calcium channel activity.

Significance Statement

This is the first study to characterise the CACHD1 protein. CACHD1 is widely expressed in the CNS, in particular in the thalamus, hippocampus and cerebellum. CACHD1 distribution is similar to that of low-voltage-activated (Ca_V3, T-type) calcium channels, in particular to $Ca_V3.1$, a protein which regulates neuronal excitability and is a potential therapeutic target in conditions such as epilepsy and pain. CACHD1 is structurally a $\alpha2\delta$-like protein that functionally increases Ca_V3 calcium current. CACHD1 increases the presence of $Ca_V3.1$ at the cell surface, forms complexes with $Ca_V3.1$ at the cell-surface and causes an increase in channel open probability. In hippocampal neurons, CACHD1 causes increases in neuronal firing. Thus, CACHD1 represents a novel protein that modulates Ca_V3 activity.

Introduction

The putative CACHD1 gene was identified following a systematic search for proteins with structural homology to α2δ VGCC auxiliary subunits. The human CACHD1 gene on chromosome 1p31.3 encodes the putative protein CACHD1 and has many orthologs, including in speciation as early as *C. elegans* (tag-180*)* and *D. melanogaster* (CG16868) (Anantharaman and Aravind, 2000). Despite only a 13-16% gene homology and a <21% protein identity with the α2δ VGCC auxiliary subunits, there are several key structural similarities between CACHD1 and α2δ in terms of the arrangement of protein motifs. α2δ and $Ca_V\beta$ subunits are described as auxiliary or accessory VGCC subunits that modulate cell-surface expression and biophysical properties of high-voltage-activated (HVA) Ca_V1 (L-type Ca^{2+} current) and Ca_V2 (P/Q, N- and R-type Ca^{2+} current) VGCC major α1 subunits (Dolphin, 2012; Dolphin, 2013). In particular, α2δ subunits are proposed to associate with HVA channels within the secretory pathway to promote plasma membrane trafficking and, consequentially, to contribute to synaptic abundance (Dolphin, 2012), transmitter release (Hoppa et al., 2012) and to defining the extent of the active zone (Schneider et al., 2015). α2δ-1 and α2δ-2 represent molecular targets of gabapentinoid drugs (Dooley et al., 2007). However, modulation of low-voltage-activated (LVA) Ca_V3 family (T-type Ca^{2+} current) by existing α2δ and $Ca_V\beta$ auxiliary subunits has not been firmly established (Dolphin et al., 1999; Lacinová et al., 1999; Dubel et al., 2004). LVA currents are activated by small depolarization to regulate excitability around the resting membrane potential and Ca_V3 channels have been proposed as therapeutic targets in diseases such as epilepsy and pain (Perez-Reyes, 2003; Cheong and Shin, 2013; Powell et al., 2014; Snutch and Zamponi, 2017); therefore, knowledge of proteins that modulate Ca_V3 activity is paramount.

Here, we investigate the novel CACHD1 protein and test the hypothesis that CACHD1 represents an α2δ-like protein that modulates Ca_V3 channels. We have previously reported that, by contrast to α2δ, the CACHD1 subunit has no clear effect on $Ca_V2.2$ biophysical properties when co-expressed together with β2a in expression system studies (Soubrane *et al*., 2012). We characterise the expression of the CACHD1 gene in rat and human tissue at the transcriptional and translational level, and demonstrate that CACHD1, but not α2δ-1, increases Ca_V3 (T-type) current density and maximal conductance. CACHD1 increases $Ca_V3.1$ channel levels at the plasma membrane and data were consistent with CACHD1 forming complexes with $Ca_V3.1$ at the cell surface to increase channel open probability. We further demonstrate that CACHD1 expression causes a functional increase in T-type current-mediated excitability in hippocampal neurons. Together, these data demonstrate that CACHD1 is structurally an α2δ-like protein which functionally modulates Ca_V3 activity.

Materials and Methods

RNA isolation and real-time polymerase chain reaction (PCR)

Tissue samples were dissected from 5 adult male Wistar rats (Harlan, UK) following isofluorane overdose and cervical dislocation, according to Home Office Animals (Scientific procedures) Act 1986, UK. Total RNA was extracted using an RNeasy kit (Qiagen, UK) with an on-column DNase I treatment. Additional total RNA samples from AMS Biotechnology (Abingdon, UK) originated from human male donors aged 24-65. RNA (500 ng) was reverse-transcribed and relative quantification of CACHD1 and $\alpha2\delta$-1 transcripts was performed using SYBR green and custom-made validated primers. HPRT1 was used as housekeeping gene. Absolute quantification of CACHD1, $\alpha2\delta$-1, -2, -3, $Ca_V2.2$ and Ca_V1, -2, -3 transcripts was evaluated using 'Best Coverage' Taqman probes (Applied Biosystems, UK) against a standard curve of plasmids containing human CACHD1 and a rat single stranded DNA standard curve.

Sample preparation for *in situ* hybridization and immunohistochemistry

Rat tissue was kindly donated by Dr Emilio Russo, University Magna Grecia of Catanzaro, Italy. Briefly, 6-month-old male rats were sacrificed by i.p. injection of pentobarbital (200 mg/kg) according to ARRIVE guidelines and local ethical approval committee of the University of Catanzaro and perfused-fixed with 4% PFA in RNAse-free PBS, pH 7.3. Brain tissue was extracted, post-fixed overnight in 4% PFA in RNAse-free PBS and then cryoprotected in 30% sucrose. After being processed to wax (Tissue-tek VIP), 5 µm horizontal plane brain slices were cut using a microtome (Leica, UK).

In situ hybridization

A CACHD1 probe consisting of a cocktail of short 10-20bp oligonucleotides spanning ~1kb was designed by ACDBio (USA) and *in situ* hybridization was performed on 5 μm rat brain sections using a RNAscope 2.0 FFPE-Red kit. Positive (POLR2A) and negative (DapB) probes were run in parallel.

Immunohistochemistry

Chromogenic immunohistochemistry was performed using antigen retrieval in citrate buffer (Thermo, UK) for 10 min and 3,3`-diaminobenzidine (DAB) staining (ImmPACT, Vector Labs, UK), dehydrated and mounted with DPX. Rabbit anti-CACHD1 (1:500) (Abcam, UK Cat #AB75141, RRID: AB_1310016) with horseradish peroxidase-coupled anti-rabbit IgG (ImmPRESS, Vector Labs, UK) was used to detect CACHD1 protein. Qualitative expression of mRNA was evaluated with a brightfield microscope according to colour intensity of labelled mRNA.

Antibodies for biochemistry

The following antibodies were used: mouse anti-HA.11 (Cambridge Bioscience, UK; clone 16B12; Lot No. B220767, RRID: AB_10063630); rabbit anti-Na+/K+-ATPase (Novus Biologicals, Abingdon, UK; NB100-80005, Lot No. YH02206, RRID: AB_2063297); mouse anti-c-Myc (Sigma-Aldrich Cat# M4439, clone 9E10, Lot No. 087M4765V, RRID: AB_439694), rabbit anti-c-Myc (Sigma-Aldrich Cat# C3956, Lot No. 016M4762V, RRID: AB_439680), mouse anti-β-actin (Sigma-Aldrich Cat# A5441, Lot No. 028K4826, RRID: AB_476744) and rabbit anti-CACHD1 (Sigma-Aldrich Cat# AV49592, Lot No. QC22258, RRID: AB_1852421); goat anti-mouse or rabbit IgG coupled to horseradish peroxidase

(Stratech Scientific Limited, Newmarket, UK); donkey anti-mouse or rabbit coupled to AlexaFluor488, 555 or 647 (Invitrogen, Paisley, UK). Note: We experienced vial-to-vial variation with the rabbit anti-CACHD1 antibody for Western blotting during this study. Although both vials were from the same Lot No. and specifically recognised CACHD1, the vial used for Fig. 4D gave rise to more non-specific staining on HEK cell lysates than vial used for Fig. 4A.

Vectors and vector construction

The human CACHD1 construct was purchased from Origene (Rockville, MA, USA) and the truncated clone completed by PCR. The subsequent open reading frame was then subcloned into pcDNA5/FRT. An N-terminal Myc tag was inserted after the natural signal sequence between Ala^{35}-Glu^{36} using standard PCR techniques. All constructs were sequenced to confirm identity. Construction of the vector pcDNA5/FRT-HA-CLR-Myc-RAMP1 has been described elsewhere (Cottrell et al., 2007).

Cell maintenance and propagation

HEK293 tsA201 (HEK) cells were cultured in DMEM (Invitrogen, UK) containing 10% fetal bovine serum (Biosera, UK) and maintained in 95% air, 5% CO_2 at 37 °C.

Cell-surface biotinylation

HEK cells were transiently transfected in 6 well plates using 3 µg DNA (ratio 2:1, GFP-Ca_V3.1-HA:CACHD1) using Lipofectamine^{2000} (3:8, DNA:Lipofectamine^{2000}). HEK cells transfected with empty vector (vector control, VC), VC + Myc-CACHD1, GFP-Ca_V3.1-HA + VC or GFP-Ca_V3.1-HA + Myc-CACHD1 were washed (3x PBS), incubated with 0.3 mg/ml

EZ-Link™-Sulfo-NHS-Biotin (Pierce, USA) in PBS (1 h, 4°C), washed (3x PBS) and cells lysed in RIPA buffer (50 mMTris/HCl, pH 7.4, 150 mM NaCl, 5 mM $MgCl_2$, 1 mM EGTA, 10 mM NaF, 10 mM $Na_4P_2O_7$, 0.1 mM Na_3VO_4, 0.5% Nonidet P-40, peptidase inhibitor cocktail (Roche, UK)), and centrifuged. Biotinylated proteins were recovered by incubation with NeutrAvidin-agarose (30 µl, overnight, 4°C), pelleted, washed with RIPA buffer (3x 1 ml), boiled in Laemmli buffer and analyzed by SDS-PAGE and Western blotting.

SDS-PAGE and Western blotting

Immunoprecipitations and whole cell lysates were separated by SDS-PAGE (6-9% acrylamide), proteins transferred to PVDF membranes (Immobilon-P, Millipore, UK) and blocked for 1 h at room temperature (1x PBS, 0.1% $Tween^{20}$, 5% non-fat milk powder [blocking buffer]). Membranes were incubated with antibodies to HA (1:5,000), β-actin (1:20,000), CACHD1 (1:1000), rabbit or mouse Myc (1:5000) or Na^+-K^+-ATPase (1:20,000) (overnight, 4°C; blocking buffer). Membranes were washed for 30 min (1x PBS, 0.1% $Tween^{20}$) and incubated with appropriate secondary antibodies coupled to horseradish peroxidase (1:10,000, 1 h, room temperature; blocking buffer). Immunoreactive proteins were detected using enhanced chemiluminescence (BioRad, UK). Densitometric analysis was performed using an ImageQuant-RT ECL imaging system (GE Healthcare, Chalfont St Giles, UK) and analysed using ImageQuant TL software.

Immunofluorescent detection of cell-surface proteins

HEK cells were transiently transfected in 12 well plates using 1 µg DNA (ratio 2:1, GFP-Ca_V3.1-HA:Myc-CACHD1) using polyethylenimine (PEI; 1:2, DNA:PEI). HEK cells transfected with empty vector (vector control, VC), VC + Myc-CACHD1, GFP-Ca_V3.1-HA +

VC, GFP-$Ca_V3.1$-HA + Myc-CACHD1 or CLR•RAMP1 seeded onto coverslips and used for experimentation after 48 h. Cells were washed twice with PBSCM, incubated in DMEM containing 0.1% BSA and mouse anti-HA (1:100) and rabbit anti-c-Myc (1:500) antibodies (1 h, 4°C), washed twice again with PBSCM and then fixed in 100 mM PBS containing 4% paraformaldehyde (w/v), pH 7.4 (20 min, 4ºC). Coverslips were incubated in blocking buffer (1x PBS, 2% normal horse serum, 0.1% saponin) (30 min, room temperature (RT)) and then incubated with appropriate secondary antibodies (1:2000, 2 h, RT). Coverslips were washed (blocking buffer, 30 min, RT) and mounted using Vectashield containing DAPI.

Proximity ligation assays

HEK cells were transiently transfected in 12 well plates using 1 μg DNA (ratio 2:1, GFP-$Ca_V3.1$-HA:Myc-CACHD1) using polyethylenimine (PEI; 1:2, DNA:PEI). HEK cells transfected with empty vector (vector control, VC), VC + Myc-CACHD1, GFP-$Ca_V3.1$-HA + VC, GFP-$Ca_V3.1$-HA + Myc-CACHD1 or CLR•RAMP1 seeded onto coverslips and used for experimentation after 48 h. Cells were washed twice with PBSCM, incubated in DMEM containing 0.1% BSA and mouse anti-HA (1:100) and rabbit anti-c-Myc (1:500) antibodies (1 h, 4°C), washed twice again with PBSCM and then fixed in 100 mM PBS containing 4% paraformaldehyde (w/v), pH 7.4 (20 min, 4ºC). After washing with PBSCM the proximity ligation assay was conducted according to the manufacturer's instructions (Duolink® In Situ Red Starter Kit Mouse/Rabbit, Cat No. DUO92101, Sigma). Briefly, cells were blocked (1 h, 37ºC), washed twice (5 min, room temperature) and then incubated with appropriate secondary antibodies (1 h, 37ºC). After washing (2x 5 min, room temperature), the ligation was conducted (30 min, 37°C) and the cells were washed twice more. Coverslips were then incubated with the amplification reaction mixture (100 min, 37°C), washed and coverslips mounted in medium containing DAPI.

Confocal microscopy

Cells were observed with a Nikon Eclipse Ti laser-scanning confocal microscope using a 100x/1.45 Oil DIC N2 objective. Images were collected at a zoom of 1-2 and at least five optical sections were taken at intervals of 0.5 µm. Single sections are shown. Images were processed using Adobe Photoshop and the NIS-Elements AR software.

Transformed human embryonic kidney cell culture and transfection for electrophysiology

For electrophysiology experiments, HEK cells were transfected using 4 µl Fugene6 (Promega, UK) with total 2 µg pcDNA3 at 50:1:25 for $Ca_V3.1$/pmaxGFP, $Ca_V3.2$/pmaxGFP or $Ca_V3.3$/pmaxGFP with or without α2δ-1 or CACHD1. Empty vector was used to compensate when α2δ or CACHD1 was omitted. Cells were maintained at 95% air, 5% CO_2 at 37 °C and used for experimentation 24-48 h post transfection**.**

Hippocampal neuron culture and transfection

Low-density hippocampal cultures were prepared from male and female E19 rat embryos as described previously (Zhang et al., 2003). All experiments were carried out in compliance with the Guide for the Care and Use of Laboratory Animals of the National Institutes of Health and approved by the University of Virginia Animal Care and Use Committee and adhered to ARRIVE guidelines. Neurons were plated onto poly-L-lysine coated glass coverslips at a density of ~70 cells/mm^2 and were transfected using lipofectamine 2000 at a ratio of 2 μl lipofectamine 2000 per 1 μg DNA. Neurons were transfected with either CACHD1 or pcDNA3.1 at a ratio of 10:1 excess to mVenus and moved 24 h after transfection to a new glia-feeder layer.

Electrophysiology

Recordings from HEK cells were made as described previously (Vogl et al., 2015). Current-voltage (I-V) relationships from individual cells were fitted with a modified Boltzmann equation: $I = G_{max}\,\mathrm{x}(V-V_{rev}) / (1 + \exp(-(V - V_{1/2})/k))$ where, G_{max} is the maximal conductance (nS/pF), $V_{1/2}$ is the midpoint of activation i.e. the voltage at which 50% of the channels are open, V_{rev} is the null potential and k is the slope factor. Tail currents (measured at -120 mV) were normalised to the maximal and minimal conductance and the resultant curves were fitted with following Boltzmann function: $I=I_0+((I_{max}-I_0)/(1+\exp(V_{1/2}-V)/k)))$. Throughout, all comparative electrophysiological experiments were performed in transfection-matched cultures.

Recordings from hippocampal neurons were performed as described previously (Jones et al., 2007). Throughout, data are expressed as mean S.E.M. Methods to estimate the probability of channel opening, Po have been previously described by us (Shcheglovitov et al., 2008), which assumes no change in single channel current, reducing the relationship between whole-cell current (I) to $I \approx NPo$, where N is the number of channels in a cell and Po is the probability of channel opening. N is estimated by measuring the channel gating current at the reversal potential for ionic current. The peak current represents the maximal gating charge Q_{max}, and is proportional to N. Peak ionic current conductance, G_{max}, was determined by fitting the I–V curve, obtained from the same cell, with a Boltzmann-Ohm equation as described earlier. G_{max} is used as a proxy for I since it is not affected by changes in driving force. Therefore, the G_{max}/Q_{max} ratio can be used to estimate Po.

Experimental Design and Statistical Analysis

Throughout, all animal studies comply to appropriate ARRIVE and NIH guidelines and comply to country and institute guidelines (as specified in Methods section for each animal study). Details of animal strain, sex and method of sacrifice and use of anaesthetics are also stated in Methods section for each animal study.

Throughout, all comparative biochemical and electrophysiological experiments were performed against transfection-matched culture controls. For electrophysiological experiments in recombinant cells, a minimum of 5 separate transfections were performed and numbers of individual replications are specified in appropriate Table. In all cases, sample size is stated in text, Figure legend or appropriate Table. Data subjected to statistical comparisons were assessed for assumptions of normality using a D'Agostino-Pearson omnibus test and expressed as mean ± standard error of the mean (SEM) throughout. Groups were compared by two-tailed paired or unpaired Student's *t*-test, Mann-Whitney test, one- or two-way ANOVA tests followed by Bonferroni post-hoc tests, Kruskal-Wallis test and Dunn's multiple comparison test or least squares fits compared using extra sum of squares F test as appropriate, using GraphPad Prism. In all cases, the statistical test used is stated in text, Figure legend or appropriate Table. Throughout, $P<0.05$ was taken as statistically significant and where appropriate values of $P<0.01$ and $P<0.001$ are specified.

Results

The novel CACHD1 protein is an α2δ paralog

We first investigated the predicted protein domain structure of CACHD1. Figure 1*A* illustrates that, like α2δ-1, CACHD1 has a predicted exofacial N-terminus according to its signal sequence, a von Willebrand factor A (VWA) domain, two bacterial chemosensory-like cache domains and a short hydrophobic transmembrane domain followed by an intracellular C-terminus. Although CACHD1 and α2δ share limited amino acid sequence homology (<21%), the similarities in modular domain content and arrangement between the proteins suggested the possibility that CACHD1 represents an α2δ-like protein. However, there are also a number of differences between CACHD1 and α2δ-1; these include: (i) α2δ proteins are a single gene product which is post-translationally cleaved by proteases into α2 and δ components and then associate via disulphide bonding (Calderon-Rivera et al., 2012; Segura et al., 2017); an important 6 amino acid motif for proteolytic cleavage has been identified (Andrade et al., 2007) which is absent in CACHD1. (ii) CACHD1 has a single predicted post-translational N-glycosylation site, whilst α2δ-1 is heavily glycosylated at multiple potential sites (Douglas et al., 2006). (iii) CACHD1 has a variant RSR amino acid sequence at the binding site for gabapentinoids. (iv) Despite expressing a VWA domain, the functionally important MIDAS motif in CACHD1 (DxGxS) is different from that of α2δ-1 (DxSxS). (v) α2δs have a predicted GPI-anchoring site (Davies et al., 2010) which is absent in CACHD1, which instead has a predicted transmembrane domain and a larger intracellular C-terminus domain.

CACHD1 is highly expressed in brain hippocampal and thalamic regions

To obtain comparative and quantitative data on CACHD1 mRNA expression, real-time PCR was performed on rat and human mRNA from different regions of the brain and peripheral tissue. Relative expression profiles of CACHD1 and α2δ-1 transcripts in rat tissue showed high CACHD1 expression in thalamus, hippocampus and cerebellum, whilst α2δ-1 transcript expression was prominent in cortex, hippocampus and also, superior cervical ganglia (Fig. 1*B*). We further investigated the anatomical distribution of CACHD1 at the transcriptional and protein levels using *in situ* hybridization and immunohistochemistry in adult mammalian brain. Rat brain regions displaying high mRNA include the hippocampus, anterodorsal thalamic nucleus, reticular thalamic nucleus, cerebellum, subiculum, medial entorhinal cortex and zona incerta (Fig. 1-1; Fig. 1-2). Hippocampal CACHD1 mRNA staining was strong in the dentate gyrus, as well as the CA1 pyramidal cell layer; mRNA staining was less strong in CA3. There was strong correlation between the levels of expression of CACHD1 mRNA and protein in rat brain (Fig. 1-2). In the thalamus, CACHD1 protein showed differential expression between major thalamic nuclei, in particular with prominent staining in the anterodorsal and reticular nuclei (Fig. 2). In human tissue, CACHD1 transcripts were similarly high in hippocampus, thalamus, and cerebellum (Fig. 2-1). CACHD1 transcript distribution was broadly similar to certain Ca_V3 subtypes, in particular to $Ca_V3.1$ (Fig. 2-1, Talley et al., 1999). CACHD1 transcript expression showed a differential distribution to α2δ-1 and α2δ-2 subtypes and was most similar to α2δ-3 (Fig. 2-1, Cole et al., 2005). In human tissue, CACHD1 protein levels were most abundant in dentate gyrus granule cells and pyramidal cells of the hippocampus cornus ammonis, cortical regions and thalamus, in both large diameter and small diameter cells (Fig. 3).

CACHD1 promotes cell-surface expression of $Ca_V3.1$

Our expression data indicated high levels of CACHD1 expression in the thalamus, hippocampus and cerebellum. As expression levels of Ca_V3 subunits are also high in the thalamus and hippocampus, we hypothesized that CACHD1 may modulate Ca_V3 subunits in a recombinant HEK cell system. As a first step, we expressed CACHD1 in HEK cells and confirmed the specificity of the CACHD1 antibody (Fig. 4*A*). Immunoreactive CACHD1 was detected at approximately 170 kDa. We also confirmed that CACHD1 is present at the cell-surface of HEK cells (Fig. 4*B*). Next, we determined if expression of CACHD1 affected the subcellular localization of $Ca_V3.1$ using a cell-surface biotinylation assay. Cell-surface proteins from HEK cells expressing empty vector, empty vector + CACHD1, GFP-$Ca_V3.1$-HA + empty vector and GFP-$Ca_V3.1$-HA + CACHD1 were extracted and levels of GFP-$Ca_V3.1$-HA analysed by Western blotting. Our data show that co-expression of CACHD1 increased cell-surface localization of GFP-$Ca_V3.1$-HA (2.65 ± 0.40 fold over control $P<0.05$ two-tailed paired Student's *t*-test; Fig. 4*C*). We also quantified the whole-cell expression of GFP-$Ca_V3.1$-HA in the same HEK cells, normalising to levels to β-actin (Fig. 4*D*). Importantly, our data shows that CACHD1 increases levels of GFP-$Ca_V3.1$-HA at the cell-surface without affecting the total cellular level.

CACHD1 and $Ca_V3.1$ are in close proximity at the cell-surface

To determine if $Ca_V3.1$ and CACHD1 are present in a complex at the cell-surface, an epitope-tagged CACHD1 (Myc-CACHD1) was used to aid cell-surface precipitation and detection. First, we tested the expression of the tagged protein and examined the ability of an anti-Myc antibody to bind to CACHD1 at the cell-surface. Myc-CACHD1 was expressed in HEK cell with a similar molecular mass (~170 kDa) to untagged CACHD1 (Fig. 5-1). Furthermore, we could detect Myc-CACHD1 at the cell-surface using immunofluorescence and confocal microscopy (Fig. 5-1). Proximity ligation assays are commonly used to predict the likelihood that two proteins are sufficiently close enough to be present in the same complex. First, we determined if we could simultaneously detect Myc-CACHD1 and GFP-Ca_V3.1-HA at the cell-surface by confocal microscopy. Live HEK cells expressing empty vector, empty vector + CACHD1, GFP-Ca_V3.1-HA + empty vector and GFP-Ca_V3.1-HA + CACHD1 were incubated with antibodies to the Myc and HA epitope tags of CACHD1 and Ca_V3.1, respectively and immunoreactive proteins visualized by immunofluorescence (Fig. 5*A*). No immunoreactive signals were detected in cells expressing empty vector, indicating antibody specificity. We were able to detect immunoreactive Myc signals only in cells expressing Myc-CACHD1. Similarly, we were able to detect signals for the HA antibody only in cells expressing GFP, indicating expression of GFP-Ca_V3.1-HA. We were also able to simultaneously detect CLR and RAMP1 at the cell-surface of transfected cells (Fig. 5*A*). Next, we labelled cells from the same transfections and performed a proximity ligation assay and visualized the cells using confocal microscopy. No PLA signals were detected in cells transfected with empty vector, empty vector + CACHD1, GFP-Ca_V3.1-HA + empty vector (Fig. 5*B*). By contrast, we could readily detect PLA signals in our positive control (CLR•RAMP1) and in transfected with GFP-Ca_V3.1-HA + CACHD1. Importantly, we could only detect PLA signals in cells expressing GFP (Fig. 5*B*). Thus, CACHD1 and Ca_V3.1 are in close proximity (<40 nm) at the cell-surface of HEK cells, indicating that they are likely in the same protein complex. As discussed more fully below, together, these data are consistent with CACHD1 increasing the cell-surface localization of Ca_V3.1 and with formation of CACHD1-Ca_V3.1 complexes at the cell surface.

CACHD1 modulates recombinant Ca_V3 family VGCCs

We next tested the hypothesis that CACHD1 modulates T-type Ca^{2+} current. Co-expression of CACHD1 with $Ca_V3.1$ caused an increase in current density around peak values (Fig. 6*A,B*) and a corresponding increase in maximal conductance (Fig. 6*B* inset; Table 1). By contrast, in our hands, $Ca_V3.1$ peak current and conductance was not modulated by α2δ-1 in transfection-matched experiments (Fig. 6*A,C*; Table 1). CACHD1 effects were not accompanied by any overall change in the midpoint of activation or slope factor k (Table 1) and CACHD1 had no effect on $Ca_V3.1$ steady-state inactivation (data not shown). Neither CACHD1 nor α2δ-1 affected $Ca_V3.1$ recovery from inactivation, as measured by lack of effect on mid-time of recovery from inactivation or $\tau_{recovery}$ ($p>0.1$ for both, one-way ANOVA with Bonferroni post-hoc test, data not shown).

We next investigated potential modulation of $Ca_V3.2$ and $Ca_V3.3$ by CACHD1. Peak current density of $Ca_V3.2$ (Fig. 7*A,C*) and $Ca_V3.3$ (Fig. 7*B*,*D*) was increased by CACHD1 with corresponding increases in maximal conductance (Table 1). CACHD1 had no significant effect on midpoint of activation or slope factor k for either $Ca_V3.2$ or $Ca_V3.3$ (Table 1) or steady-state inactivation ($p>0.1$, Kruskal-Wallis test with Dunn's multiple comparison test, data not shown). CACHD1 was without effect on Ca_V3 activation or inactivation kinetics (Fig. 7-1; Table 1). In our hands, α2δ-1 was without effect on current density in $Ca_V3.2$ (Fig. 7*E*) or $Ca_V3.3$ (Fig. 7*F*). α2δ-1 was without effect on $Ca_V3.2$ activation kinetics or on $Ca_V3.2$ and $Ca_V3.3$ inactivation kinetics (Fig. 7-1; Table 1). α2δ-1 had subtle effects on $Ca_V3.1$ activation and inactivation kinetics and $Ca_V3.3$ activation kinetics (Fig. 7-1; Table 1). Overall, these data suggest that CACHD1, but not α2δ-1, has a major effect on recombinant Ca_V3 VGCCs in terms of increased Ca^{2+} current density and maximal conductance.

To determine the mechanism by which CACHD1 increased T-type channel currents, we estimated channel opening probability by measuring $Ca_V3.1$ gating currents at the reversal potential for the ionic current (Fig. 8). In these experiments, the CACHD1-mediated increase in current density was recapitulated; thus, $Ca_V3.1$ maximal conductance 280 ± 30 pS/pF was significantly increased to 860 ± 15 pA/pF (n = 12 for each condition from 3 separate transfections; $P<0.001$ Mann-Whitney test) (data not shown). Measurement of area under the gating current provides a measure of the maximal gating charge Q_{max}. A plot of conductance versus gating current amplitude of the ionic current of the same cell provides a measure of open probability (Po) (Agler et al., 2005). Under these conditions, there was a ~1.4 fold increase in $Ca_V3.1$ Po in CACHD1 expressing cells ($P<0.001$, Fig. 8). These findings are consistent with CACHD1 interaction with $Ca_V3.1$ at the cell surface causing a functional increase in Po as a major contribution to CACHD1-mediated increases in Ca^{2+} current density.

CACHD1 increase Ca_V3-mediated excitability in hippocampal neurons

Ca_V3 channels are predicted to affect neuronal excitability around the resting membrane potential (Perez-Reyes, 2003; Cheong and Shin, 2013). To investigate the role of CACHD1 in controlling neuronal excitability, we expressed CACHD1 (vs. empty vector controls) in hippocampal neurons. Transfected neurons were identified by co-expression of the biomarker mVenus (Fig. 9*A*). At a depolarizing current injection step of 220 pA, CACHD1 expressing neurons fired at a higher frequency than control neurons (Fig. 9*B,C,D;* Table 2). To further determine the role of T-type currents in establishing the increase in neuronal firing frequencies, we used the selective Ca_V3 channel blocker, TTA-P2 (Dreyfus et al., 2010). TTA-P2 (1 μM) reversed the firing frequency in CACHD1 expressing neurons back to control levels, but was without effect on control neurons (Fig. 9*D;* Table 2). To increase the contribution of T-type current to neuronal excitability, a hyperpolarizing prepulse was used to recover LVA Ca^{2+} channels from inactivation, followed by a short depolarizing pulse to evoke an AP (Eckle et al., 2014). Under these conditions, CACHD1 expression caused a more profound increase in rebound firing frequency in CACHD1-transfected, but not control, neurons (Fig. 9*E,F,G;* Table 2). TTA-P2 (1 μM) reversed the increase in rebound AP firing in CACHD1 expressing neurons back to control levels, but was without effect on control neurons (Fig. 9*G;* Table 2). Throughout these experiments, CACHD1 had no significant effects on AP waveform properties (Fig. 9-1). These data support a CACHD1-mediated selective increase in T-type Ca^{2+} current, which leads to an increase in AP firing frequency and excitability in native neurons.

Discussion

This study characterises the protein CACHD1, encoded by the cache domain containing 1 gene, and presents evidence that it represents a novel protein that modulates Ca_V3 VGCC activity. These data also provide further evidence that the major $\alpha2\delta$-1 auxiliary calcium channel subunit does not fulfil a similar role for Ca_V3 channels. Detailed examination of $Ca_V3.1$ channels suggests an underlying mechanism whereby CACHD1 promotes increased $Ca_V3.1$ levels at the plasma membrane. In addition, data were consistent with CACHD1 forming a complex with the channel at the cell surface to increase open probability and potentiate T-type current.

CACHD1 protein modulates Ca_V3 VGCCs

At a cellular level, CACHD1 transcripts were localised to granule and pyramidal cells of the hippocampus, and specific thalamic nuclei, notably the anterodorsal thalamic nucleus and reticular nucleus. Compared to the gene expression of the major $\alpha2\delta$-1 and $\alpha2\delta$-2 subunits, CACHD1 protein displayed a unique expression signature with, in particular, high expression in the thalamus and hippocampus and also in some regions of the cerebellum and cortex. CACHD1 was largely co-incident with the expression pattern of the $Ca_V3.1$ channel in the CNS (Talley et al., 1999). CACHD1 co-transfection with $Ca_V3.1$ in recombinant cells increased cell surface expression and Ca^{2+} current levels and maximal conductance. CACHD1 similarly modulated $Ca_V3.2$ and $Ca_V3.3$ current levels. Under equivalent conditions, $\alpha2\delta$-1 was without significant effect on current levels in any Ca_V3 subtype. Proximity ligation assays were consistent with CACHD1 being able to form complexes with $Ca_V3.1$ at the cell surface. Mechanistically, CACHD1 effects on $Ca_V3.1$ were associated with increases in channel Po. A similar role has been reported for $\alpha2\delta$ auxiliary subunit interactions with Ca_V1 channels; thus, α2δ-1 increased channel Po and channel number as well as allosterically regulating drug binding (Shistik et al., 1995; Wei et al., 1995). Other studies have reported either an α2δ-mediated reduction in Po (Wakamori et al., 1999) or a lack of effect on Po (Brodbeck et al., 2002). The latter study suggested that α2δ predominantly performs a VGCC trafficking function to increase the number of active channels at the membrane (reviewed by Dolphin, 2012). The demonstrated CACHD1-mediated increase in $Ca_V3.1$ cell surface expression is proposed to contribute to increase in cell Ca^{2+} current levels and maximal conductance. Here, the ~1.4-fold increase in Po is insufficient to fully account for the ~3 fold increase in current density seen in this set of experiments; channel number is predicted to increase (according to I= iNPo, where I is the whole-cell current, i is the single channel current (predicted to be constant) and N is the number of functional channels). Thus, increase in channel number may be attributable to either CACHD1-mediated increases in forward trafficking or reduced endocytosis of $Ca_V3.1$. With respect to α2δ auxiliary subunits, HVA Ca_Vα1- α2δ interactions are reported to occur during early maturation at an intracellular site to drive forward trafficking to the plasma membrane (Cantí et al., 2005). Whilst $Ca_V2.2$ proteomic data have reported only a low appreciable amount of co-purified α2δ, with detection dependent on solubilising agent used (Müller et al., 2010), recent work using exofacial tags and antigen stripping techniques has supported α2δ also remaining associated with $Ca_V2.2$ at the plasma membrane (Cassidy et al., 2014). In the present study, clear indication of CACHD1 and Cav3.1 complex formation at the cell surface was obtained using proximity ligand assays. Moreover, α2δ has the propensity to sequester into lipid raft compartments, as reported by us (Ronzitti et al., 2015) and others; this may also limit efficient detection of α2δ-Ca_Vα1 complexes and it will be of interest to determine if CACHD1 similarly localizes to lipid rafts. Overall, we propose that

CACHD1 acts to increase Ca_V3 expression at the plasma membrane, at the cell surface CACHD1 can form a complex with the channel to increase Po and, consequentially, increase T-type current.

Potential functional impact of CACHD1 on Ca_V3 VGCCs

T-type Ca^{2+} currents are active around the resting membrane potential, where non-inactivating channels generate low threshold Ca^{2+} spikes and the consequential triggering of Na^+-dependant APs (Llinás 1988; Cheong and Shin, 2013). Of further interest here is that multiple mechanisms and proteins involved in folding and trafficking are reported to be involved in Ca_V3 expression at the cell surface. For example, proteins such the actin binding protein kelch-like 1 (Aromomolaran et al., 2010), stac1 (Rzhepetskyy et al., 2016) and calnexin (Proft et al., 2017) have a proposed role in Ca_V3 expression. Moreover, the glycosylated form of Ca_V3 represents the mature, correctly folded protein that is associated with higher Po (Weiss et al., 2013; Ondacova et al., 2016). T-type current has also been implicated in regulating presynaptic transmitter release in hippocampal and nociceptive circuitry (Huang et al., 2011; Jacus et al., 2012). Increases in Ca_V3 current are predicted to have profound effects on neuronal firing (McCormick and Huguenard, 1992). Correspondingly, over-expression of CACHD1 caused a pronounced increase in T-type current-mediated spike firing in hippocampal neurons. This activity was enhanced using a protocol to trigger recovery of Ca_V3 channels from their inactivated states, thereby increasing contribution of T-type current to neuronal excitability. Ca_V3 subtypes have been suggested as targets for anti-epileptic drugs (Powell et al., 2014). In models of temporal lobe epilepsy (TLE), selective up-regulation of T-type current in hippocampal neurons causes intrinsic bursting activity (Sanabria et al., 2001; Su et al., 2002). $Ca_V3.2$ transcripts were upregulated in TLE models and intrinsic burst firing was reduced in $Ca_V3.2$ knock-out mice (Becker et al., 2008). Moreover, the deubiquitinating enzyme USP5 (Garcia-Callero et al., 2014), and preventing $Ca_V3.2$ deubiquitination was suggested to be beneficial in neuropathic and inflammatory pain. Our data suggest CACHD1 as a potential future target in hyperexcitability disorders associated with Ca_V3 dysfunction, such as epilepsy and pain. Moreover, CACHD1 gene expression has been shown to be modulated in patients with Type 1 diabetes (Rassi et al., 2008) and Parkinson's disease (Aguiar and Severino, 2010).

CACHD1 protein structure dictates α2δ-like function

There are clear similarities in protein structural motifs between CACHD1 and α2δ, namely, the presence of an N-terminal signal sequence, VWA and two downstream cache domains, these similarities suggest a conserved evolution (Anantharaman and Aravind, 2000). However, a number of important differences are also present. CACHD1 has a RSR variant at the gabapentin binding motif; whilst α2δ-1 and α2δ-2 were found to bind to gabapentinoids via their RRR binding motif, α2δ-3 and α2δ-4 have variant RNR sites which do not bind gabapentin (Wang et al., 1999; Marais et al., 2001). Earlier studies also identified porcine α2δ-1 residues 516 to 537 within the first cache domain and residues 583 to 603 as also contributing to gabapentin binding (Wang et al., 1999). It will be of interest to determine if CACHD1 binds gabapentanoids. Despite sharing a common VWA domain, CACHD1 has a variant MIDAS motif. The α2δ-1 MIDAS motif is functionally important in Ca^{2+} channel trafficking and synaptic function (Cantí et al., 2005; Hoppa et al., 2012). However, it has been suggested that MIDAS is unlikely to represent a key $Ca_V2.2$/α2δ-1 interaction site, rather other regions are more likely involved (Cassidy et al., 2014); such regions may include cache domains, for example, rat α2δ-1 residues 751-755, which are within a modelled cache region, were implicated in $Ca_V2.2/\alpha2\delta$-1 interaction (Cassidy et al., 2014). By contrast, comparative data investigating α2δ effects on $Ca_V1.2$ point to aspartate and the first serine residue within the DxSxS MIDAS site as molecular determinants for interaction and correct modulation of $Ca_V1.2$ (Briot et al., 2018). Of interest here is that CACHD1 contains a variant MIDAS with a glycine residue at the equivalent position of the critical serine residue identified by Briot et al. (2018). It has also been proposed that the α2δ amino terminal (amino acids 26-230, termed the R-domain) contains all the machinery required to support α2δ-1-mediated current enhancement in $Ca_V2.2$ channels (Song et al., 2015). This study identified a tryptophan residue (W205), which is conserved across all four α2δ isoforms, as an important molecular determinant for these R-domain effects; it is of note that CACHD1 also contains a conserved tryptophan residue at the equivalent position.

In bacteria, the cache domain is proposed to arise from bacterial small molecule binding domains PAS and GAF (Anantharaman et al., 2001) and to play a key role in chemotaxis by acting as an extracellular receptor (Anantharaman and Aravind, 2000). Recent computational work has suggested that cache domains represent the dominant extracellular sensor in prokaryotes; by contrast, cache domains are largely limited to only α2δ subunits in metazoa (Upadhyay et al., 2016). The present study adds CACHD1 to this classification. Whilst the functional relevance of mammalian cache domains remains to be fully established, deletions within the cache domain of α2δ-4 have been associated with familial bipolar disorder (Van Den Bossche et al., 2010). Roles for 'free' α2δ (not associated with VGCCs) have also been extended to functions including synaptogenesis and neurodegeneration via interaction with alternative ligands such as thrombospondins and prion proteins, respectively (Eroglu et al., 2009, Lana *et al*., 2016; Senatore et al., 2012); it will also be of interest to see if CACHD1 possesses similar functionality.

Overall, our data are consistent with CACHD1 structurally representing an α2δ-like protein that act to increase Ca_V3 cell surface expression and current. Identification of the CACHD1 protein as a modulator of Ca_v3 activity expands the range of VGCC associated proteins and may provide an additional target itself, or via its modulation of T-type current, in different disease states.

References

Agler HL, Evans J, Tay LH, Anderson MJ, Colecraft HM, Yue DT (2005) G protein-gated inhibitory module of N-type (Ca_V2.2) Ca^{2+} channels. Neuron 46:891-904.

Aguiar PM, Severino P (2010) Biomarkers in Parkinson Disease: global gene expression analysis in peripheral blood from patients with and without mutations in PARK2 and PARK8. Einstein (Sao Paulo) 8:291-297.

Anantharaman V, Aravind L (2000) Cache - a signaling domain common to animal Ca^{2+}-channel subunits and a class of prokaryotic chemotaxis receptors. Trends Biochem Sci 25:535-537.

Anantharaman V, Koonin EV, Aravind L (2001) Regulatory potential, phyletic distribution and evolution of ancient, intracellular small-molecule-binding domains. J Mol Biol 307: 1271-1292.

Andrade A, Sandoval A, Oviedo N, De Waard M, Elias D, Felix R (2007) Proteolytic cleavage of the voltage-gated Ca^{2+} channel $\alpha2\delta$ subunit: structural and functional features. Eur J Neurosci 25:1705-1710.

Aromolaran KA, Benzow KA, Cribbs LL, Koob MD, Piedras-Rentería ES (2010) T-type current modulation by the actin-binding protein Kelch-like 1. Am J Physiol Cell Physiol 298:C1353–1362.

Baumgart JP, Vitko I, Bidaud I, Kondratskyi A, Lory P, Perez-Reyes E (2008) I-II loop structural determinants in the gating and surface expression of low voltage-activated calcium channels. PLoS ONE 3:e2976.

Becker AJ, Pitsch J, Sochivko D, Opitz T, Staniek M, Chen CC, Campbell KP, Schoch S, Yaari Y, Beck H (2008) Transcriptional upregulation of Cav3.2 mediates epileptogenesis in the pilocarpine model of epilepsy. J Neurosci 28:13341-13353.

Briot J, Mailhot O, Bourdin B, Tétreault MP, Najmanovich R, Parent L (2018) A three-way inter-molecular network accounts for the $\mathrm{Ca_V}\alpha2\delta1$-induced functional modulation of the pore-forming $\mathrm{Ca_V}1.2$ subunit. J Biol Chem Mar 27 [Epub ahead of print].

Brodbeck J, Davies A, Courtney JM, Meir A, Balaguero N, Cantí C, Moss FJ, Page KM, Pratt WS, Hunt SP, Barclay J, Rees M, Dolphin AC (2002) The ducky mutation in Cacna2d2 results in altered Purkinje cell morphology and is associated with the expression of a truncated α2δ2 protein with abnormal function. J Biol Chem 277:7684-7693.

Calderon-Rivera A, Andrade A, Hernández-Hernández O, González-Ramírez R, Sandoval A, Rivera M, Gomora JC, Felix R (2012) Identification of a disulfide bridge essential for structure and function of the voltage-gated Ca^{2+} channel α2δ-1 auxiliary subunit. Cell Calcium 51:22–30.

Cantí C, Nieto-Rostro M, Foucault I, Heblich F, Wratten J, Richards MW, Hendrich J, Douglas L, Page KM, Davies A, Dolphin AC (2005) The metal-ion-dependent adhesion site in the Von Willebrand factor-A domain of α2δ subunits is key to trafficking voltage-gated Ca^{2+} channels. Proc Natl Acad Sci U S A 102:11230-11235.

Cassidy JS, Ferron L, Kadurin I, Pratt WS, Dolphin AC (2014) Functional exofacially tagged N-type calcium channels elucidate the interaction with auxiliary α2δ-1 subunits. Proc Natl Acad Sci U S A 111: 8979-8984.

Cheong E, Shin HS (2013) T-type Ca^{2+} channels in normal and abnormal brain functions. Physiol Rev 93:961-992.

Cole R, Lechner SM, Williams ME, Prodanovich P, Bleicher L, Varney MA, Gu G (2005) Differential distribution of voltage-gated calcium channel alpha-2 delta (α2δ) subunit mRNA-containing cells in the rat central nervous system and the dorsal root ganglia. J Comp Neurol 491:246-269.

Cottrell GS, Padilla B, Pikios S, Roosterman D, Steinhoff M, Grady EF, Bunnett NW (2007) Post-endocytic sorting of calcitonin receptor-like receptor and receptor activity-modifying protein 1. J Biol Chem 282:12260-12271.

Davies A, Kadurin I, Alvarez-Laviada A, Douglas L, Nieto-Rostro M, Bauer CS, Pratt WS, Dolphin AC (2010) The α2δ subunits of voltage-gated calcium channels form GPI anchored proteins, a posttranslational modification essential for function. Proc Natl Acad Sci U S A 107:1654–1659.

Dolphin AC, Wyatt CN, Richards J, Beattie RE, Craig P, Lee JH, Cribbs LL, Volsen SG, Perez-Reyes E (1999) The effect of α2δ and other accessory subunits on expression and properties of the calcium channel α1G. J Physiol 519:35-45.

Dolphin AC (2012) Calcium channel auxiliary α2δ and β subunits: trafficking and one step beyond. Nat Rev Neurosci 13:542-555.

Dolphin AC (2013) The α2δ subunits of voltage-gated calcium channels. Biochim Biophys Acta 1828:541-1549.

Dooley DJ, Taylor CP, Donevan S, Feltner D (2007) Ca^{2+} channel α2δ ligands: novel modulators of neurotransmission. Trends Pharmacol Sci 28:75-82.

Douglas L, Davies A, Wratten J, Dolphin AC (2006) Do voltage-gated calcium channel α2δ subunits require proteolytic processing into α2 and δ to be functional? Biochem Soc Trans 34:894-898.

Dreyfus FM, Tscherter A, Errington AC, Renger JJ, Shin HS, Uebele VN, Crunelli V, Lambert RC, Leresche N (2010) Selective T-type calcium channel block in thalamic neurons reveals channel redundancy and physiological impact of $I_{Twindow}$. J Neurosci 30:99-109.

Dubel S, Altier C, Chaumont S, Lory P, Bourinet E, Nargeot J (2004) Plasma membrane expression of T-type calcium channel α1 subunits is modulated by high voltage-activated auxiliary subunits. J Biol Chem 279:29263-29269.

Eckle V-S, Shcheglovitov A, Vitko I, Dey D, Yap CC, Winckler B, Perez-Reyes E (2014) Mechanisms by which a *CACNA1H* mutation found in epilepsy patients increases seizure susceptibility. J Physiol 592:795-809.

Eroglu C, Allen NJ, Susman MW, O'Rourke NA, Park CY, Ozkan E, Chakraborty C, Mulinyawe SB, Annis DS, Huberman AD, Green EM, Lawler J, Dolmetsch R, Garcia KC, Smith SJ, Luo ZD, Rosenthal A, Mosher DF, Barres BA (2009) Gabapentin receptor α2δ-1 is a neuronal thrombospondin receptor responsible for excitatory CNS synaptogenesis. Cell 139:380-392.

García-Caballero A,Gadotti VM, Stemkowski P, Weiss N, Souza IA, Hodgkinson V, Bladen C, Chen L, Hamid J, Pizzoccaro A, Deage M, François A, Bourinet E, Zamponi GW (2014) The deubiquitinating enzyme USP5 modulates neuropathic and inflammatory pain by enhancing Cav3.2 channel activity. Neuron 83:1144-1158.

Hoppa M, Lana B, Margas W, Dolphin AC, Ryan TA (2012) α2δ couples calcium channels to neurotransmitter release sites to control release probability. Nature 486:122–125.

Huang Z, Lujan R, Kadurin I, Uebele VN, Renger JJ, Dolphin AC, Shah MM (2011) Presynaptic HCN1 channels regulate $Ca_V3.2$ activity and neurotransmission at select cortical synapses. Nat Neurosci 14:478-486.

Jacus MO, Uebele VN, Renger JJ, Todorovic SM (2012) Presynaptic Cav3.2 channels regulate excitatory neurotransmission in nociceptive dorsal horn neurons. J Neurosci 32: 9374-9382.

Jones PJ, Wang Y, Smith MD, Hargus NJ, Eidam HS, White HS, Kapur J, Brown ML, Patel MK (2007) Hydroxyamide analogs of propofol exhibit state-dependent block of sodium channels in hippocampal neurons: implications for anticonvulsant activity J Pharmacol Exp Ther 320:828-36.

Lacinová L, Klugbauer N, Hofmann F (1999) Absence of modulation of the expressed calcium channel α1G subunit by α2δ subunits. J Physiol 516:639-645.

Lana B, Page KM, Kadurin I, Ho S, Nieto-Rostro M, Dolphin AC (2016) Thrombospondin-4 reduces binding affinity of [^{3}H]-gabapentin to calcium-channel $\alpha_2\delta$-1 subunit but does not interact with $\alpha_2\delta$-1 on the cell-surface when co-expressed. Sci Rep 6:24531

Llinás RR (1988) The intrinsic electrophysiological properties of mammalian neurons: insights into central nervous system function. Science 242:1654-1664.

Marais E, Klugbauer N, Hofmann F (2001) Calcium channel $\alpha2\delta$ subunits-structure and gabapentin binding. Mol Pharmacol 59:1243-1248.

McCormick DA, Huguenard JR (1992) A model of the electrophysiological properties of thalamocortical relay neurons. J Neurophysiol 68:1384-1400.

Müller CS, Haupt A, Bildl W, Schindler J, Knaus HG, Meissner M, Rammner B, Striessnig J, Flockerzi V, Fakler B, Schulte U (2010) Quantitative proteomics of the Cav2 channel nano-environments in the mammalian brain. Proc Natl Acad Sci U S A 107:14950-14957.

Ondacova K, Karmazinova M, Lazniewska J, Weiss N, Lacinova L (2016) Modulation of Cav3.2 T-type calcium channel permeability by asparagine-linked glycosylation. Channels (Austin) 10:175–184.

Perez-Reyes E (2003) Molecular physiology of low-voltage-activated T-type calcium channels. Physiol Rev 83:117-161.

Powell KL, Cain SM, Snutch TP, O'Brien TJ (2014) Low threshold T-type calcium channels as targets for novel epilepsy treatments. Br J Clin Pharmacol 77:729-739.

Proft J, Rzhepetskyy Y, Lazniewska J, Zhang FX, Cain SM, Snutch TP, Zamponi G, Weiss N (2017) The Cacna1h mutation in the GAERS model of absence epilepsy enhances T-type Ca^{2+} currents by altering calnexin-dependent trafficking of $Ca_V3.2$ channels. Sci Rep 7:11513.

Rassi DM, Junta CM, Fachin AL, Sandrin-Garcia P, Mello S, Silva GL, Evangelista AF, Magalhães DA, Wastowski IJ, Crispim JO, Martelli-Palomino G, Fernandes AP, Deghaide NN, Foss-Freitas MC, Foss MC, Soares CP, Sakamoto-Hojo ET, Passos GA, Donadi EA (2008) Gene expression profiles stratified according to type 1 diabetes mellitus susceptibility regions. Ann N Y Acad Sci 1150:282-289.

Ronzitti G, Bucci G, Emanuele M, Leo D, Sotnikova TD, Mus LV, Soubrane CH, Dallas ML, Thalhammer A, Cingolani LA, Mochida S, Gainetdinov RR, Stephens GJ, Chieregatti E (2014) Exogenous α-synuclein decreases raft partitioning of Cav2.2 channels inducing dopamine release. J Neurosci 34:10603-10615.

Rzhepetskyy Y, Lazniewska J, Proft J, Campiglio M, Flucher BE, Weiss N (2016) A $Ca_V3.2$/Stac1 molecular complex controls T-type channel expression at the plasma membrane. Channels (Austin) 10:346–354.

Sanabria ER, Su H, Yaari Y (2001) Initiation of network bursts by Ca^{2+}-dependent intrinsic bursting in the rat pilocarpine model of temporal lobe epilepsy. J Physiol 532:205-216.

Schneider R, Hosy E, Kohl J, Klueva J, Choquet D, Thomas U, Voigt A, Heine M (2015) Mobility of calcium channels in the presynaptic membrane. Neuron 86:672-679.

Segura E, Bourdin B, Tétreault MP, Briot J, Allen BG, Mayer G, Parent L (2017) Proteolytic cleavage of the hydrophobic domain in the $Ca_V\alpha2\delta1$ subunit improves assembly and activity of cardiac $Ca_V1.2$ channels. J Biol Chem 292:11109-11124.

Senatore A, Colleoni S, Verderio C, Restelli E, Morini R, Condliffe SB, Bertani I, Mantovani S, Canovi M, Micotti E, Forloni G, Dolphin AC, Matteoli M, Gobbi M, Chiesa R (2012) Mutant PrP suppresses glutamatergic neurotransmission in cerebellar granule neurons by impairing membrane delivery of VGCC α2δ-1 subunit. Neuron 74:300-313.

Shcheglovitov A, Vitko I, Bidaud I, Baumgart JP, Navarro-Gonzalez MF, Grayson TH, Lory P, Hill CE, Perez-Reyes E (2008) Alternative splicing within the I-II loop controls surface expression of T-type $Ca_V3.1$ calcium channels. FEBS Lett 582, 3765–3770.

Shistik E, Ivanina T, Puri T, Hosey M, Dascal N (1995) Ca^{2+} current enhancement by α2/δ and β subunits in Xenopus oocytes: contribution of changes in channel gating and α1 protein level. J Physiol 489:55-62.

Snutch TP, Zamponi GW (2017) Recent advances in the development of T-type calcium channel blockers for pain intervention. Br J Pharmacol Jun 13 [Epub ahead of print].

Song L, Espinoza-Fuenzalida IA, Etheridge S, Jones OT, Fitzgerald EM (2015) The R-domain: Identification of an N-terminal region of the α2δ-1 subunit which is necessary and sufficient for its effects on $Ca_V2.2$ calcium currents. Curr Mol Pharmacol 8:169-179.

Soubrane CH, Stevens EB, Stephens GJ (2012) Expression and functional studies of the novel CNS protein CACHD1. Physiology 2012 (Edinburgh) Proc Physiol Soc 27, PC74.

Su H, Sochivko D, Becker A, Chen J, Jiang Y, Yaari Y, Beck H (2002) Upregulation of a T-type Ca^{2+} channel causes a long-lasting modification of neuronal firing mode after status epilepticus. J Neurosci 22:3645-3655.

Talley E, Cribbs LL, Lee JH, Daud A, Perez-Reyes E, Bayliss DA (1999) Differential distribution of three members of a gene family encoding low voltage-activated (T-type) calcium channels. J Neurosci 19:1895-1911.

Upadhyay AA, Fleetwood AD, Adebali O, Finn RD, IB ZN (2016) Cache domains that are homologous to, but different from PAS domains comprise the largest superfamily of extracellular sensors in prokaryotes. PLoS Comput Biol 12:e1004862.

Van Den Bossche MJ, Strazisar M, De Bruyne S, Bervoets C, Lenaerts AS, De Zutter S, Nordin A, Norrback KF, Goossens D, De Rijk P, Green EK, Grozeva D, Mendlewicz J, Craddock N, Sabbe BG, Adolfsson R, Souery D, Del-Favero J (2012) Identification of a CACNA2D4 deletion in late onset bipolar disorder patients and implications for the involvement of voltage-dependent calcium channels in psychiatric disorders. Am J Med Genet B Neuropsychiatr Genet 159B:465-475.

Vogl C, Tanifuji S, Danis B, Daniels V, Foerch P, Wolff C, Whalley BJ, Mochida S, Stephens GJ (2015) Synaptic vesicle glycoprotein 2A modulates vesicular release and calcium channel function at peripheral sympathetic synapses. Eur J Neurosci 41:398-409.

Wakamori M, Mikala G, Mori Y (1999) Auxiliary subunits operate as a molecular switch in determining gating behaviour of the unitary N-type Ca^{2+} channel current in Xenopus oocytes. J Physiol 517:659-72.

Wang M, Offord J, Oxender D, Su T (1999) Structural requirement of the calcium-channel subunit $\alpha 2\delta$ for gabapentin binding. Biochem J 342:313-320.

Wei X, Pan S, Lang W, Kim H, Schneider T, Perez-Reyes E, Birnbaumer L (1995) Molecular determinants of cardiac Ca^{2+} channel pharmacology. Subunit requirement for the high affinity and allosteric regulation of dihydropyridine binding. J Biol Chem 270:27106-27111.

Weiss N, Black SA, Bladen C, Chen L, Zamponi GW (2013) Surface expression and function of Cav3.2 T-type calcium channels are controlled by asparagine-linked glycosylation. Pflugers Arch 465:1159-1170.

Zhang H, Webb DJ, Asmussen H, Horwitz AF (2003) Synapse formation is regulated by the signaling adaptor GIT1. J Cell Biol 161:131-142.

Figure Legends

Figure 1. Predicted protein sequence homology and relative expression profile of CACHD1 and α2δ-1.

CACHD1 and α2δ-1 subunits both contain a N-terminus signal peptide, a VWA domain, two cache domains, and transmembrane and intracellular domains. GBP: gabapentin binding domain (RRR). GBP*: gabapentin binding domain variant (RSR). MIDAS: metal-ion-dependent adhesion site (DxSxS). MIDAS*: metal-ion-dependent adhesion site variant (DxGxS). VWA: von Willebrand factor A. Cache: Ca^{2+} channel and chemotaxis receptor. TM: transmembrane domain. Cys: cysteine. His: histidine (locations of domains are approximate and from data from www.Uniprot.org, figure drawn using DOG: Domain Graphics). (B) Relative expression profile of CACHD1 and α2δ-1 mRNA in rat tissue determined using SYBR green real-time quantitative PCR and HPRT1 as housekeeping gene. DRG: dorsal root ganglion. SCG: superior cervical ganglion. (Data normalised to lowest tissue expression; n=3 experiments using 3 animals each). Figure 1 is supported by *in situ* hydridization data in different rat brain regions (Fig. 1-1) and qualitative expression profile of CACHD1 mRNA and protein in the adult rat brain (Fig. 1-2).

Figure 2. CACHD1 protein expression in adult rat brain.

Immunoreactive protein was detected using rabbit anti-CACHD1 with peroxidase anti-rabbit secondary antibody and DAB staining (brown). AD: anterodorsal thalamic nucleus; AVDM: anteroventral thalamic nucleus (dorsomedial); AVVL: anteroventral thalamic nucleus (ventro-lateral); fi: fimbria; MD: mediodorsal thalamic nucleus; Po: posterior thalamic nucleus; sm: strai medullaris; Rt: reticular thalamus nucleus; RtSt: reticular VL: ventrolateral thalamic nucleus; VPL: ventro-posterior lateral thalamus; g: granule cell layer; m: molecular layer; p: Purkinje cell; wm: white matter. Figure 2 is supported by expression profiling of CACHD1 and different voltage-gated calcium channel subunit mRNA in human tissue (Fig. 2-1).

Figure 3. CACHD1 protein expression in human brain.

Immunohistochemistry of adult human brain using rabbit anti-CACHD1 with peroxidase anti-rabbit secondary antibody with (brown) DAB stain. CA1-3: cornus ammonis 1-3; DG: dentate gyrus.

Figure 4. Characterisation of CACHD1 and its effects on $Ca_V3.1$ channel expression.

HEK cells were transfected with empty vector (vector control, VC), CACHD1, Myc-CACHD1, GFP-$Ca_V3.1$-HA alone or in combination, as shown in each panel. (A) HEK cell lysates were analysed by Western blotting (WB). An antibody to CACHD1 recognised a single protein similar to the predicted size for CACHD1, but also recognized a non-specific protein in all lysates. (B) Cell-surface proteins were biotinylated and pull downs analysed for CACHD1 and Na^+/K^+-ATPase (loading control). In control cells, no immunoreactive CACHD1 was detected, confirming antibody specificity. In CACHD1 expressing cells, immunoreactive CACHD1 was detected. In both cell types, immunoreactive Na^+/K^+-ATPase was detected. (C) Cell-surface proteins were biotinylated and pull downs analysed for GFP-$Ca_V3.1$-HA (HA) and Na^+/K^+-ATPase (loading control). In control cells and cells only expressing CACHD1, no HA signals were detected, confirming antibody specificity. In cells expressing GFP-$Ca_V3.1$-HA, HA signals were readily detected. Quantification of the HA signals (normalised to Na^+/K^+-ATPase) revealed expression of CACHD1 increased signals for GFP-$Ca_V3.1$-HA at the cell-surface, *$p<0.05$. Na^+/K^+-ATPase signals were detected in all cell types (D) Inputs of the biotin pull down assays were analysed by WB. Signals for HA were only detected in cells expressing GFP-Ca$_V$3.1-HA, signals for CACHD1 were only detected in cells expressing Myc-CACHD1 and signals for β-actin were detected in all cell types. All blots are representative of n≥3 experiments.

Figure 5. Ca$_V$3.1 and CACHD1 are present at the cell-surface and are in close proximity. Live HEK cells expressing empty vector (vector control, VC), VC + Myc-CACHD1, GFP-Ca$_V$3.1-HA + VC, Myc-CACHD1 + GFP-Ca$_V$3.1-HA or CLR•RAMP1 (positive control) were incubated with antibodies to HA and Myc, washed and fixed. (A) Cells were then incubated with appropriate secondary antibodies and immunoreactive proteins localised by immunofluorescence and confocal microscopy. In HEK-VC cells, no signals for GFP, HA or Myc were detected indicating specificity of detection. HA signals (arrowheads) were only detected in cells expressing GFP-Ca$_V$3.1-HA (as determined by the GFP signal) and CLR•RAMP1. Similarly, Myc signals (yellow arrowheads) were only detected in cells expressing Myc-CACHD1 and CLR•RAMP1. Scale bar, 10 µm (B) After the proximity ligation assay, no signals were detected in cells expressing empty vector or in cells expressing only Myc-CACHD1 or GFP-Ca$_V$3.1-HA. In contrast, PLA signals were detected in cells expressing Myc-CACHD1 + GFP-Ca$_V$3.1-HA (arrows) and CLR•RAMP1 (arrows). Single optical sections are shown except for the PLA panel (CLR•RAMP1 excluded) where 5 optical sections are merged, two above and two below (0.5 µm increments) from the optical sections shown in the GFP/DAPI panel. Scale bar, 20 µm. All images are representative of n=3 experiments. Figure 5 is supported by analysis of cell-surface CACHD1 construct expression studies (Fig. 5-1).

Figure 6. Effects of CACHD1 and α2δ-1 on $Ca_V3.1$ channels

CACHD1 significantly increased current density as shown by (A) representative current density traces at -25 mV and (B) I-V relationships, V_H -90 mV (*p<0.05, **p<0.01, ***p<0.001, two-way ANOVA with Bonferroni post-hoc test). α2δ-1 had no significant effect on current density as shown by (A) representative current density traces at -25 mV and (C) I-V relationships, V_H -90 mV. CACHD1, but not α2δ-1, significantly increased maximal conductance (inset, p<0.05, one-way ANOVA with Bonferroni post-hoc test).

Figure 7. Effects of CACHD1 and α2δ-1 on $Ca_V3.2$ and $Ca_V3.3$ channels

CACHD1 significantly increased current density as shown by representative current density traces at -20 mV for (A) $Ca_V3.2$ and (C) $Ca_V3.3$, and I-V relationships for (B) $Ca_V3.2$ and (D) $Ca_V3.3$; V_H -90 mV (*p<0.05, **p<0.01, ***p<0.001, two-way ANOVA with Bonferroni post-hoc test). α2δ-1 had no effect on (E) $Ca_V3.2$ and (F) $Ca_V3.3$ I-V relationships, V_H -90 mV. Figure 7 is supported by analysis of effects of CACHD1 and α2δ-1 on Ca_V3 channel kinetic properties (Fig. 7-1).

Figure 8. CACHD1 expression increases $Ca_V3.1$ gating currents and open probability (Po).

Representative gating currents recorded from $Ca_V3.1$ (Aa) and $Ca_V3.1$ + CACHD1 (Ab) at the observed reversal potential. Expanded time scale illustrates the increase in area under the gating current for CACHD1 expressed cells. B) Conductance vs gating current plot for multiple cells. Line represents linear regression to data points. The slopes (G_{max}/Q_{max}) were significantly different (P=0.0004, least squares fits compared using extra sum of squares F test; $Ca_V3.1$: 0.09 ± 0.003, n=10, and $Ca_V3.1$ + CACHD1: 0.14 ± 0.090, n=11). C) Plot showing the slopes (i.e relative Po) and S.E.M. for fits shown in B (***p<0.001).

Figure 9. Effects of CACHD1 in hippocampal neurons

(A) Co-labelling of hippocampal neurons with CACHD1 and mVenus. (B) CACHD1 increased firing frequency of hippocampal neurons. (C) Example traces in response to depolarizing current injections steps of -20, 70 and 140 pA. (D) Summary data from separate experiments confirming CACHD1-mediated increased firing frequency and also showing that TTA-P2 (1 μM) reduced firing rates in CACHD1-expressing neurons, but not in controls. (E) Rebound APs were evoked using a -50 pA hyperpolarizing prepulse followed by a depolarizing step from 0 pA to 200 pA in steps of 10 pA for 200 ms, CACHD1 expressing neurons displayed a significantly greater number of rebound APs compared to controls. (F) Example traces representing depolarizing current injection steps of 40, 90 and 140 pA. (G) Summary data from separate experiments confirming CACHD1-mediated increased in rebound APs and also showing that TTA-P2 (1 μM) reduced firing rates in CACHD1-expressing neurons, but not in controls. *P<0.05 throughout, two-tailed paired Student's t-test or one-way ANOVA with Bonferroni post-hoc test. Figure 9 is supported by analysis of effects of CACHD1 and TTA-P2 on biophysical properties of hippocampal neurons (Fig. 9-1).

Extended Data Figure Legends

Figure 1-1: CACHD1 mRNA expression in adult rat brain.

In situ hybridization of adult rat brain. CACHD1 mRNA was labelled pink with blue counterstain (Gill's I Haematoxylin). CA1-3: cornus ammonis 1-3; DG: dentate gyrus; g: granule cell layer; m: molecular layer; p: Purkinje cell; wm: white matter.

Figure 1-2: Qualitative expression profile of CACHD1 mRNA and protein in the adult rat brain.

+ labelling similar to background; ++ weak labelling; +++ moderate labelling, ++++ strong labelling; +++++ very strong labelling.

Figure 2-1: Expression profile of CACHD1 and voltage-gated calcium channel subunit mRNA in human tissue.

Absolute quantification of CACHD1, α2δ-1, -2, -3, $Ca_V2.2$ and Ca_V1, -2, -3 transcripts was assessed in triplicate by TaqMan® qPCR using 'Best Coverage' Taqman probes (Applied Biosystems, UK) against a 5-point standard curve of plasmids consisting of 10-fold dilution of a known copy number of plasmid containing cDNA of the gene of interest. Total RNA was extracted using an RNeasy kit (Qiagen, UK) with an on-column DNase I treatment. Additional total RNA samples from AMS Biotechnology (Abingdon, UK) originated from human male donors aged 24-65.

Figure 5-1:Analysis of cell-surface CACHD1 construct expression.

(A, B) HEK cells were transfected with empty vector (vector control, VC) or Myc-CACHD1 and cell lysates analysed by (A) Western blotting (WB) and (B) immunofluorescence and confocal microscopy. (A) Immunoreactive signals for Myc (mouse Myc, mMyc) were detected at a similar molecular mass to that predicted for CACHD1 only in cells expressing

CACHD1. (B, upper panel) Cells were incubated with antibody to Myc (rabbit Myc, rMyc), washed, fixed and then incubated with appropriate secondary antibodies. Myc signals (arrowheads) were only detected in cells expressing Myc-CACHD1. (B, lower panel) Cells were fixed, incubated with antibody to Myc (rMyc), washed and then incubated with appropriate secondary antibodies. Myc signals were detected at the cell-surface (arrowheads) and in intracellular vesicles only in cells expressing Myc-CACHD1. Scale bar, 10 μm.

Figure 7-1: Effects of CACHD1 and α2δ-1 on Ca_V3 channel kinetic properties

CACHD1 co-expression had no significant effect on $t_{activation}$ in (Aa) $Ca_V3.1$, (Ba) $Ca_V3.2$ and (Ca) $Ca_V3.3$. α2δ-1 significantly increased $Ca_V3.1$ $t_{activation}$ at all voltages tested (Aa) (*p<0.05, **p<0.01, ***p<0.001, two-way ANOVA with Bonferroni post-hoc test); α2δ-1 had no effect on $Ca_V3.2$ $t_{activation}$ (Ba); α2δ-1 significantly decreased $Ca_V3.3$ $t_{activation}$ at -35 and -30 mV (Ca) (*p<0.05, ***p<0.001, two-way ANOVA with Bonferroni post-hoc test). CACHD1 co-expression had no significant effect on $t_{inactivation}$ in (Ab) $Ca_V3.1$, (Bb) $Ca_V3.2$ and (Cb) $Ca_V3.3$. α2δ-1 co-expression with $Ca_V3.1$ (Ab) resulted in significantly faster inactivation kinetics (*p<0.05, one-way ANOVA with Bonferroni post-hoc test), but had no effect on $t_{inactivation}$ in (Bb) $Ca_V3.2$ and (Cb) $Ca_V3.3$. Inactivation traces at -20 mV or -30 mV were fitted with a single exponential function.

Figure 9-1: Effects of CACHD1 and TTA-P2 on biophysical properties of hippocampal neurons.

Extended Data Fig. 9-1 supports Figure 9.

Table 1. Effects of CACHD1 and α2δ-1 on biophysical properties of $\mathrm{Ca_V}$3 subtypes.

	G_{max} (pS/pF)	**$V_{1/2}$ (mV)**	**k (mV)**	**τ activation (ms)***	**τ inactivation (ms)****
$\mathrm{Ca_V}$3.1 (18)	628 ± 70	-34.5 ± 0.8 (30)	5.4 ± 0.1 (30)	2.0 ± 0.1	25.8 ± 2.0
$\mathrm{Ca_V}$3.1/ CACHD1 (19)	944 ± 90*	-36.3 ± 0.9 (29)	5.6 ± 0.2 (29)	2.0 ± 0.2	22.2 ± 4.8
$\mathrm{Ca_V}$3.1/ α2δ-1 (13)	672 ± 90	-35.7 ± 1.4	5.6 ± 0.3	3.3 ± 0.2$^{\Delta\Delta}$	18.9 ± 0.86$^{\Delta}$
*=p<0.05 vs. $\mathrm{Ca_V}$3.1 (one-way ANOVA with Bonferroni post-hoc test) $^{\Delta}$ =p<0.05, $^{\Delta\Delta}$ =p<0.05 vs. $\mathrm{Ca_V}$3.1 (two-way ANOVA with Bonferroni post-hoc test)					
$\mathrm{Ca_V}$3.2 (13)	596 ± 120	-34.4 ± 2.4	5.7 ± 0.2	7.1 ± 0.40	33.3 ± 0.97
$\mathrm{Ca_V}$3.2/ CACHD1 (15)	1060 ± 140*	-33.4 ± 0.8	5.9 ± 0.2	5.9 ± 0.38	32.0 ± 1.6
*=p<0.05 vs. $\mathrm{Ca_V}$3.2 (two-tailed unpaired Student's *t*-test)					
$\mathrm{Ca_V}$3.3 (12)	573 ± 88	-36.1 ± 1.2	4.3 ± 0.2	24.4 ± 1.9	134 ± 12
$\mathrm{Ca_V}$3.3/ CACHD1 (10)	849 ± 78*	-38.9 ± 1.6	4.0 ± 0.3	28.5 ± 3.4	126 ± 8.3
*=p<0.05 vs. $\mathrm{Ca_V}$3.3 (two-tailed unpaired Student's *t*-test)					

In all cases, comparisons were performed in culture-matched experiments. Numbers in parenthesis represents number of cells each from a minimum of 5 separate transfections.

* τ activation was measured at -25 mV in all cases.
** τ inactivation was measured at -20 mV for $\mathrm{Ca_V}$3.1 and $\mathrm{Ca_V}$3.2 and at -30 mV for $\mathrm{Ca_V}$3.3.

Table 2. Effects of CACHD1 and TTA-P2 on hippocampal neuronal firing

	Firing frequency (Hz)	**Rebound firing frequency (Hz)**
Control	6.0 ± 1.2 (41/6)	7.2 ± 1.2 (32/5)
CACHD1	9.8 ± 1.1* (29/5)	12.1 ± 0.9* (28/5)
Control	8.5 ± 1.4 (6/3)	10.0 ± 1.8 (6/3)
Control + TTA-P2	6.5 ± 1.2 (6/3)	9.2 ± 1.5 (6/3)
CACHD1	14.1 ± 1.7 (7/3)	16.7 ± 0.8 (10/3)
CACHD1 + TTA-P2	6.9 ± 1.4* (7/3)	10.0 ± 1.2* (10/3)

*= $p<0.05$ vs control two-tailed paired Student’s *t*-test

Values represent means ± S.E.M; number in parenthesis = number of neurons/number of separate transfections.

Figure 1. Cottrell et al

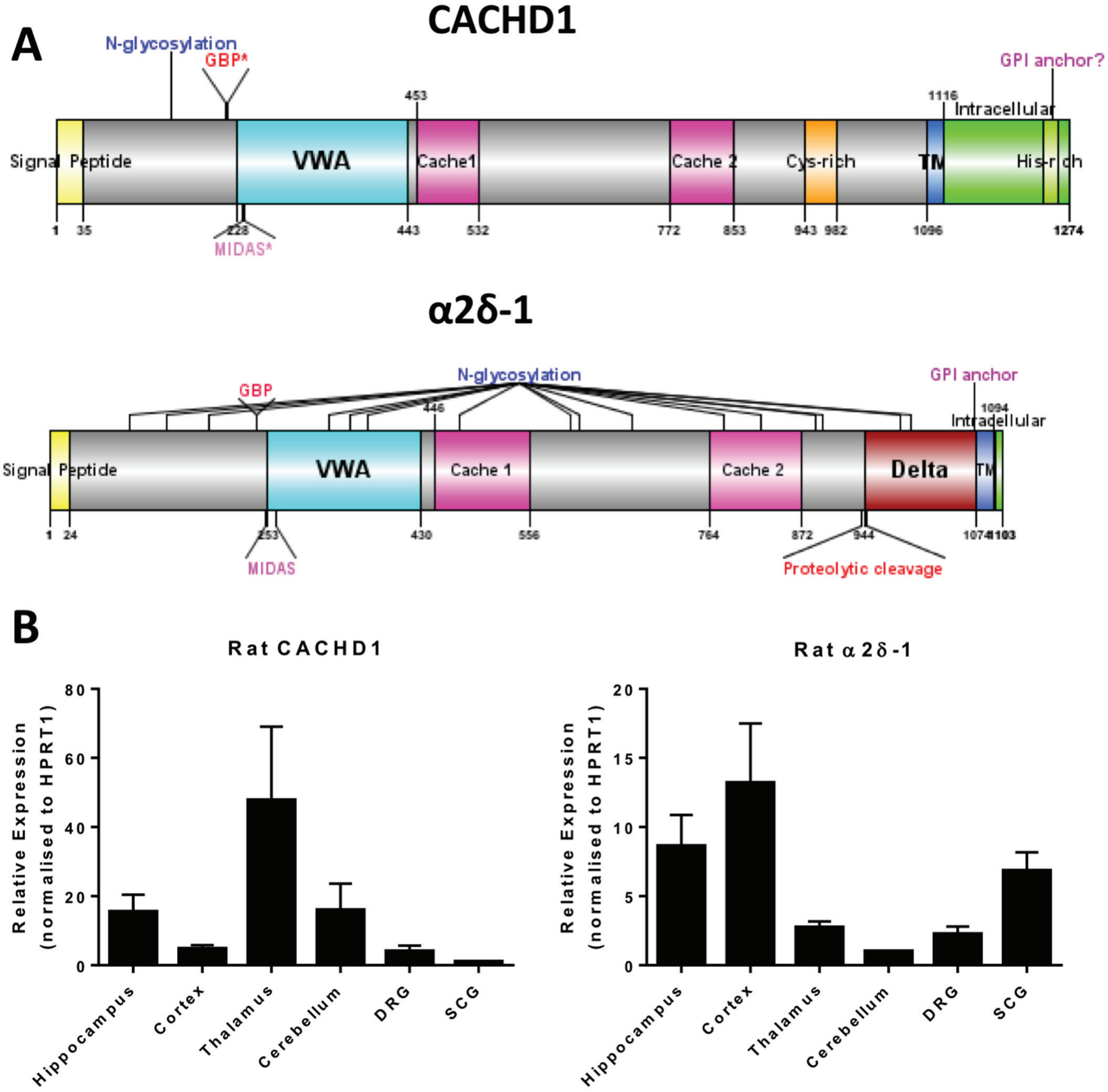

Figure 2. Cottrell et al

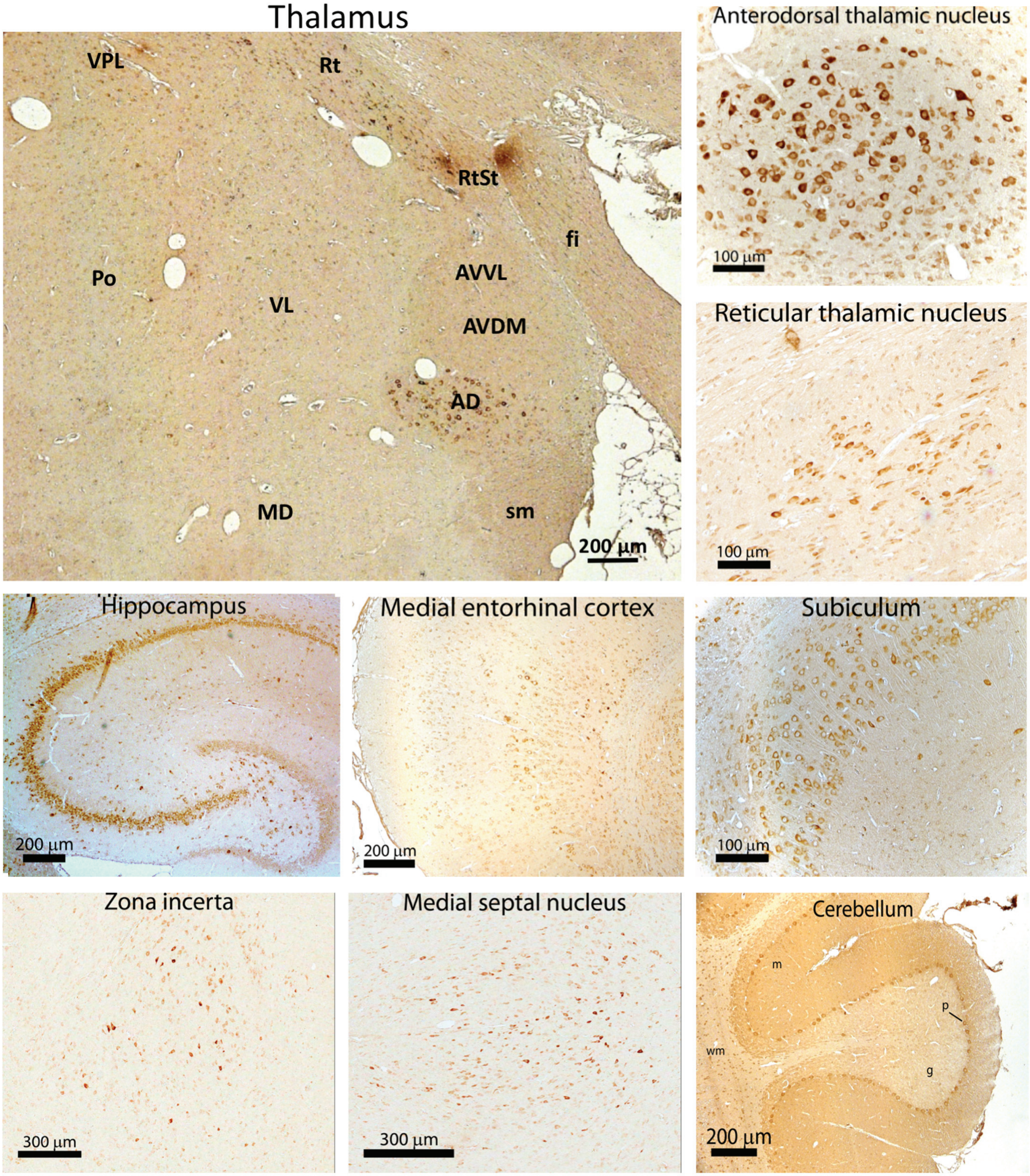

Figure 3. Cottrell et al

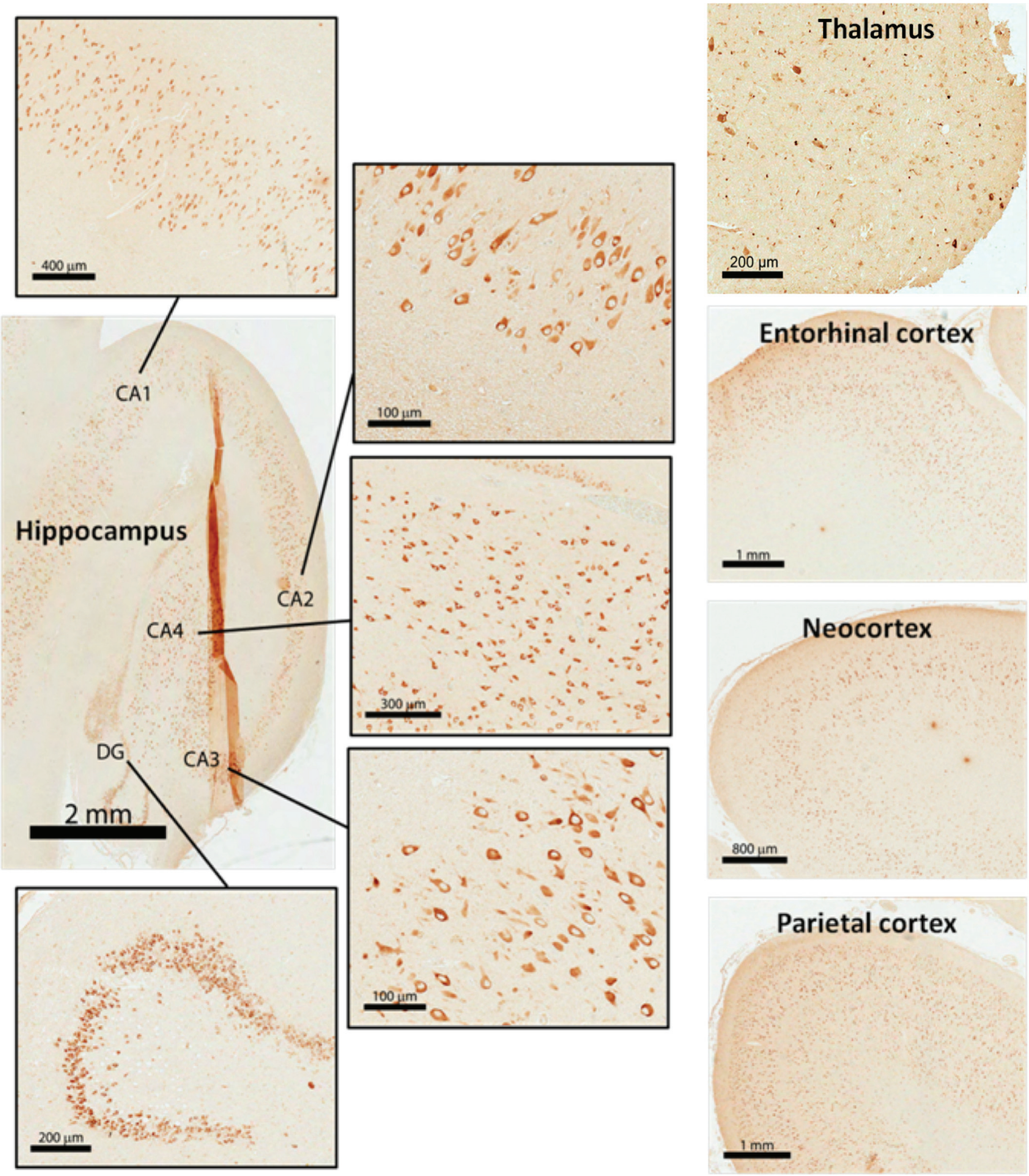

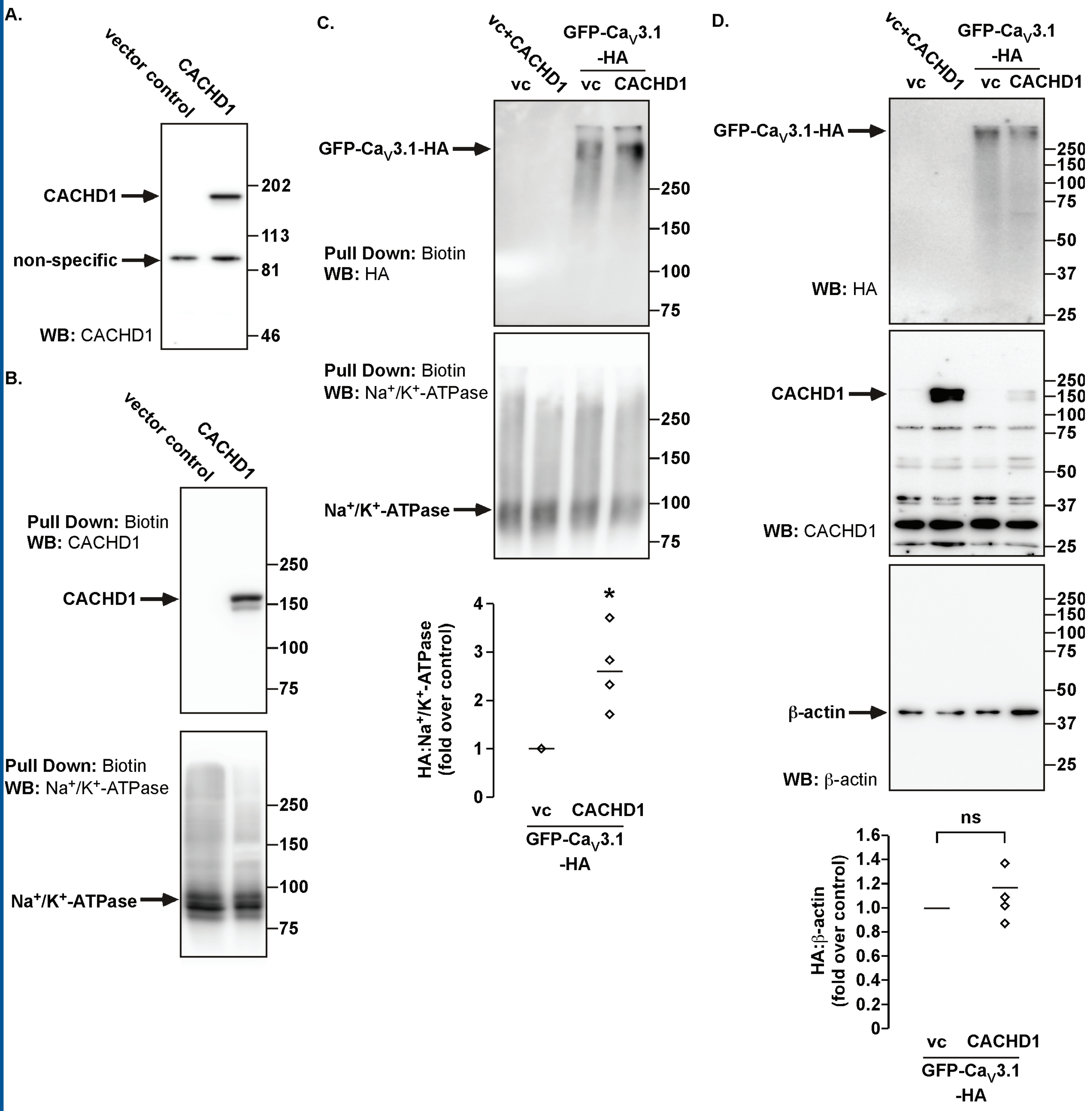
A.
vector control
CACHD1
CACHD1
non-specific
WB: CACHD1
202
113
81
46
B.
vector control
CACHD1
Pull Down: Biotin
WB: CACHD1
CACHD1
250
150
100
75
Pull Down: Biotin
WB: Na⁺/K⁺-ATPase
Na⁺/K⁺-ATPase
250
150
100
75
C.
vc+CACHD1
GFP-CaV3.1 -HA
vc
vc
CACHD1
GFP-CaV3.1-HA
Pull Down: Biotin
WB: HA
250
150
100
75
Pull Down: Biotin
WB: Na⁺/K⁺-ATPase
Na⁺/K⁺-ATPase
250
150
100
75
HA:Na⁺/K⁺-ATPase (fold over control)
0
1
2
3
4
*
vc
CACHD1
GFP-CaV3.1 -HA
D.
vc+CACHD1
GFP-CaV3.1 -HA
vc
vc
CACHD1
GFP-CaV3.1-HA
WB: HA
250
150
100
75
50
37
25
CACHD1
WB: CACHD1
250
150
100
75
50
37
25
β-actin
WB: β-actin
250
150
100
75
50
37
25
HA:β-actin (fold over control)
0
0.2
0.4
0.6
0.8
1.0
1.2
1.4
1.6
ns
vc
CACHD1
GFP-CaV3.1 -HA

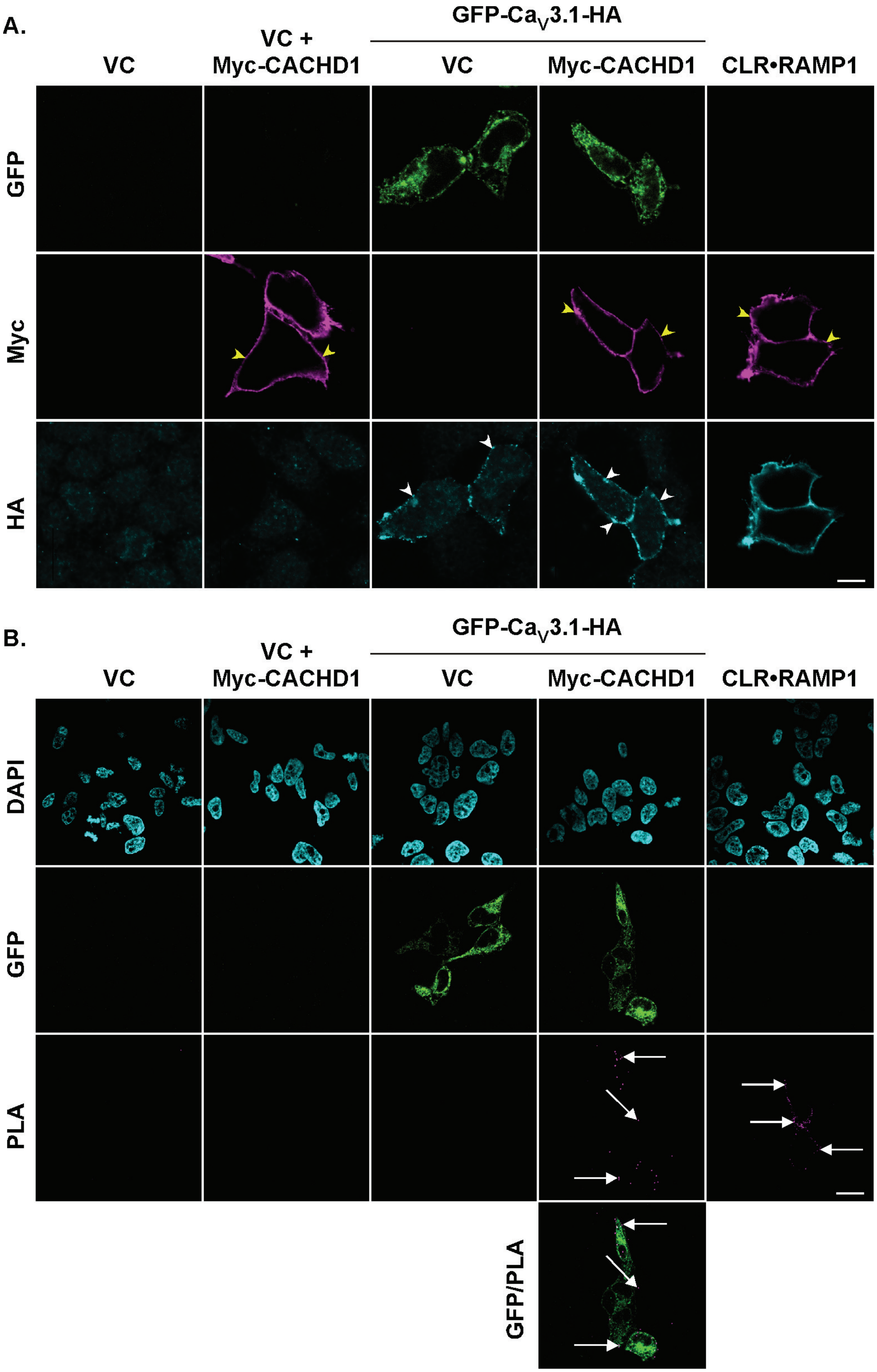
A.
GFP-Ca_V3.1-HA
VC
VC +
Myc-CACHD1
VC
Myc-CACHD1
CLR•RAMP1
GFP
Myc
HA
B.
GFP-Ca_V3.1-HA
VC
VC +
Myc-CACHD1
VC
Myc-CACHD1
CLR•RAMP1
DAPI
GFP
PLA
GFP/PLA

Figure 6. Cottrell et al

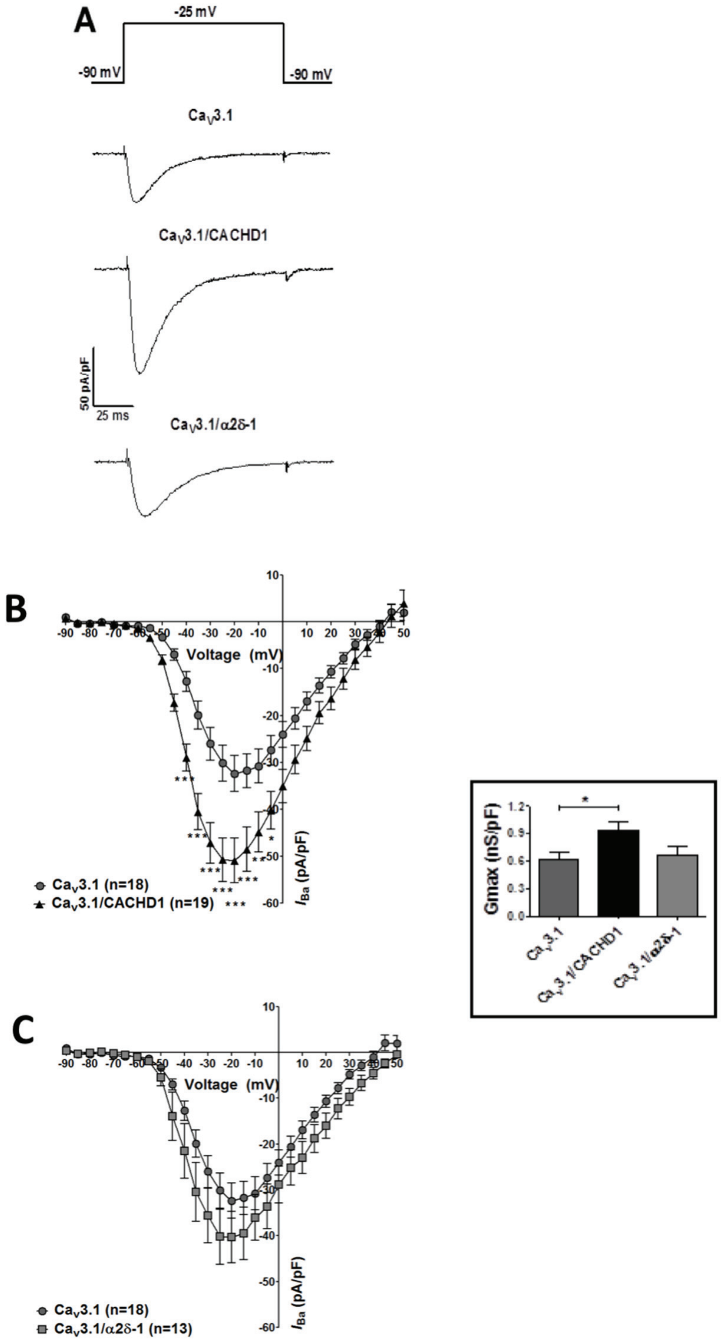

Figure 7. Cottrell et al

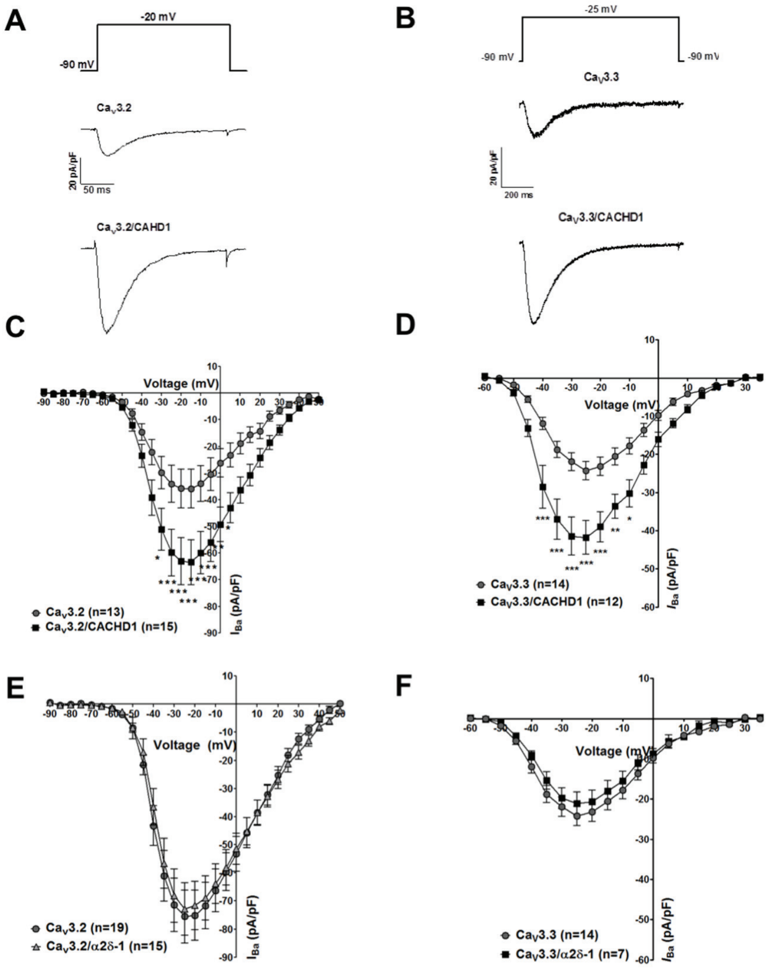

Figure 8. Cottrell et al

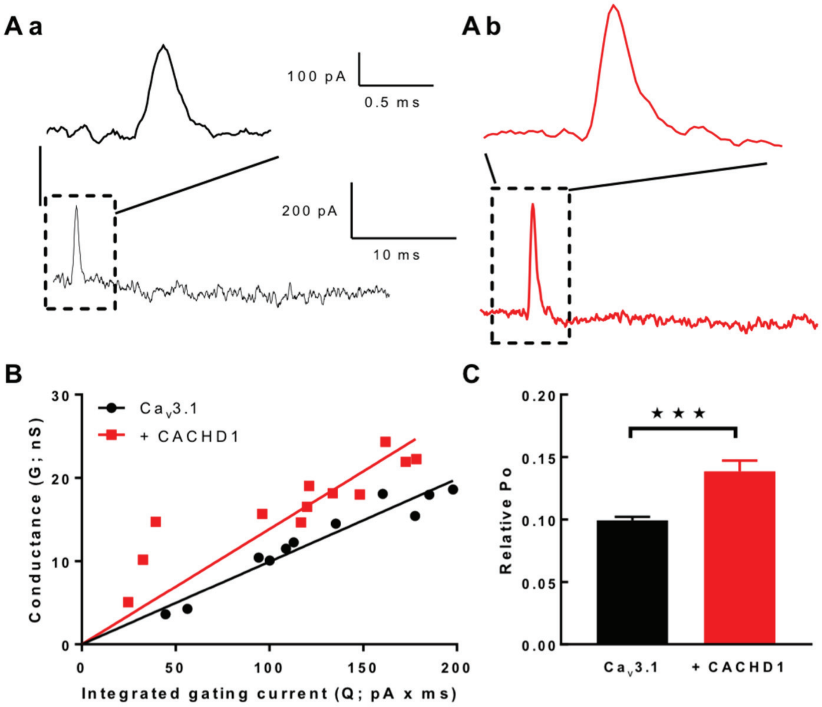

Figure 9. Cottrell et al